ELSEVIER

Contents lists available at ScienceDirect

Advanced Drug Delivery Reviews

journal homepage: www.elsevier.com/locate/adr



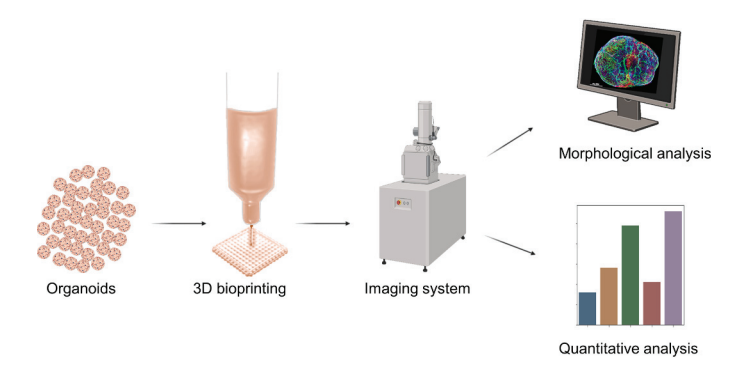


Advanced 3D imaging and organoid bioprinting for biomedical research and therapeutic applications

Sushila Maharjan ^a, Chenshuo Ma ^b, Bibhor Singh ^c, Heemin Kang ^{d,e}, Gorka Orive ^{f,g,h,i,j}, Junjie Yao ^{b,*}, Yu Shrike Zhang ^{a,*}

- a Division of Engineering in Medicine, Department of Medicine, Brigham and Women's Hospital, Harvard Medical School, Cambridge, MA 02139, USA
- ^b Department of Biomedical Engineering, Duke University, Durham, NC 27708, USA
- ^c Winthrop L. Chenery Upper Elementary School, Belmont, MA 02478, USA
- ^d Department of Materials Science and Engineering, Korea University, Seoul 02841, Republic of Korea
- ^e College of Medicine, Korea University, Seoul 02841, Republic of Korea
- f NanoBioCel Research Group, School of Pharmacy, University of the Basque Country (UPV/EHU), Vitoria-Gasteiz, Spain
- g Bioaraba, NanoBioCel Research Group, Vitoria-Gasteiz, Spain
- ^h Biomedical Research Networking Centre in Bioengineering, Biomaterials and Nanomedicine (CIBER-BBN). Vitoria-Gasteiz, Spain
- i University Institute for Regenerative Medicine and Oral Implantology UIRMI (UPV/EHU-Fundación Eduardo Anitua), Vitoria, 01007, Spain
- ^j Singapore Eye Research Institute, The Academia, 20 College Road, Discovery Tower, Singapore 169856, Singapore

GRAPHICAL ABSTRACT



$A\ R\ T\ I\ C\ L\ E\ I\ N\ F\ O$

Keywords:
Organoids
Imaging
3D bioprinting
Biofabrication
Biomedicine

ABSTRACT

Organoid cultures offer a valuable platform for studying organ-level biology, allowing for a closer mimicry of human physiology compared to traditional two-dimensional cell culture systems or non-primate animal models. While many organoid cultures use cell aggregates or decellularized extracellular matrices as scaffolds, they often lack precise biochemical and biophysical microenvironments. In contrast, three-dimensional (3D) bioprinting allows precise placement of organoids or spheroids, providing enhanced spatial control and facilitating the direct fusion for the formation of large-scale functional tissues *in vitro*. In addition, 3D bioprinting enables fine tuning of biochemical and biophysical cues to support organoid development and maturation. With advances in the organoid technology and its potential applications across diverse research fields such as cell biology,

E-mail addresses: junjie.yao@duke.edu (J. Yao), yszhang@bwh.harvard.edu (Y. Shrike Zhang).

^{*} Corresponding authors.

developmental biology, disease pathology, precision medicine, drug toxicology, and tissue engineering, organoid imaging has become a crucial aspect of physiological and pathological studies. This review highlights the recent advancements in imaging technologies that have significantly contributed to organoid research. Additionally, we discuss various bioprinting techniques, emphasizing their applications in organoid bioprinting. Integrating 3D imaging tools into a bioprinting platform allows real-time visualization while facilitating quality control, optimization, and comprehensive bioprinting assessment. Similarly, combining imaging technologies with organoid bioprinting can provide valuable insights into tissue formation, maturation, functions, and therapeutic responses. This approach not only improves the reproducibility of physiologically relevant tissues but also enhances understanding of complex biological processes. Thus, careful selection of bioprinting modalities, coupled with appropriate imaging techniques, holds the potential to create a versatile platform capable of addressing existing challenges and harnessing opportunities in these rapidly evolving fields.

1. Introduction

Organoids are miniature three-dimensional (3D) tissue structures that are grown in vitro using pluripotent stem cells (PSCs), such as embryonic stem cells (ESCs) or induced PSCs (iPSCs), tissue-specific adult stem cells (ASCs), or primary cells from healthy or diseased tissues such as tumors (Figure 1A); they serve as unique microphysiological systems with self-organization and self-renewal capabilities [1]. Organoids are produced by cell-intrinsic genetic reprogramming that are primarily triggered by meticulously chosen soluble biochemical niche signals either in suspension cell cultures or 3D extracellular matrix (ECM)-like cultures that promote the process of self-organization and tissue-specific organogenesis [2-4]. These organoids possess many tissue-resident cell types and replicate key aspects of the tissue-level morphologies and physiological functionalities of the corresponding in vivo counterparts, which are not achievable with conventional two-dimensional (2D) cultures and xenograft or transgenic animal models [5,6]. Compared to conventional 2D cultures that employ single cell-type populations without spatial organization, 3D organoids better-resemble the native microscale tissue/organ architectures with cellular heterogeneities, tissue-specific gene and protein expressions, as well as metabolic activities. On the other hand, reproducing human biology and diseases in animals can be imprecise [7]. Moreover, organoids offer greater accessibility for manipulation of multiple signaling pathways in in vivo-like microenvironments for in-depth human-based biological studies as compared to some animal models [5]. Organoids therefore provide promising in vitro tools to advance studies in the fields of tissue

development [8,9], regeneration and repair [10,11], and cell therapy [12], as well as in disease modeling [9,13-15], diagnostics [16], drug screening [17], and personalized medicine [18,19], while limiting the need for animal studies. As such, organoids have been successfully established for numerous tissues (Figure 1B), including but not limited to the gut [20-34], kidney [35-43], brain [44-65], liver [66-76], heart [77-82], mammary glands [83-89], pancreas [90-92], lung [93-103], prostate [104-110], thyroid [111-117], and retina [118-125].

Multiple techniques have been used to assess the key aspects of the organoids, such as cellular composition, morphology, molecular signature, as well as the intra- and inter-organoid heterogeneity. For example, real-time polymerase chain reaction is commonly employed for a rapid quantitative assessment of marker genes including crucial transcription factors and differentiation markers [126]. Similarly, western blotting analysis provides additional quantitative insights into relative abundances of proteins, protein-protein interactions, as well as posttranslational modifications of proteins that are indicative of the cell signaling pathways present in a particular type of cells [127,128]. Of note, the most frequently used techniques to evaluate the cellular composition and spatial distribution of cells within organoids involve the use of immunofluorescence and immunohistochemical 2D imaging of tissue sections or whole-mount samples to detect specific cell markers [129,130]. Nevertheless, compared to conventional 2D imaging of tissue sections or whole-mount samples, 3D imaging techniques offer a more efficient method of acquisition and analysis of volumetric structures of organoids for obtaining crucial information such as morphological structures, cellular compositions, cell-cell interactions, and functions of

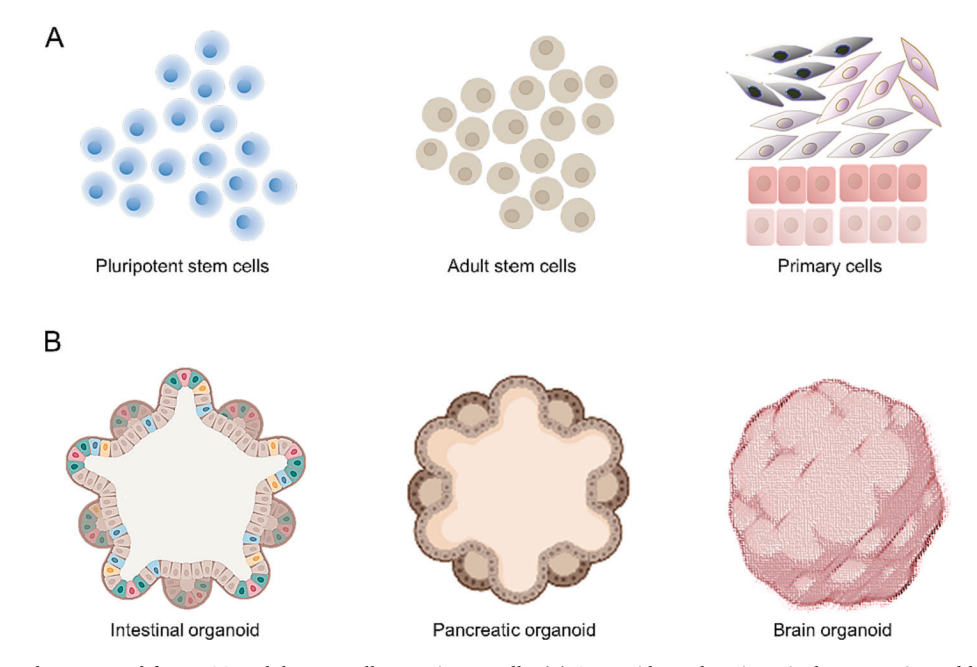


Fig. 1. (A) Organoids can be generated from PSCs, adult stem cells, or primary cells. (B) Organoids, such as intestinal, pancreatic, and brain organoids, are often generated using the conventional approach.

intact organoids [131,132]. 3D imaging offers opportunities to investigate the diverse cellular compositions, structural intricacies, and variability within or between organoids. Moreover, the use of automated 3D imaging of organoids facilitates real-time monitoring of their development, which is important for obtaining crucial information such as cell-fate specification during organogenesis, cellular compositions, cell-cell interactions and functions, as well as dynamic signaling of intact organoids in a timely manner [133,134].

While organoids serve as physiologically relevant in vitro models that are useful for investigating basic biology of organ development and disease progression as well as for creating viable tissues for transplantation and drug developments, there are several limitations of organoids that need to overcome in order to achieve their even broader biomedical applicability. Since organoids are generated by suspension cell cultures or 3D ECM-like cultures with exogenous biochemical signals that guide cells to self-assemble, they often lack precise spatiotemporal control and lead to significantly heterogeneous organoids with varying levels of cellular composition, shape, and size [1]. Efforts have been made for attaining improved regulation or enrichment of specific cell populations, largely by refining biochemical cues while inducing lineage-specific tissue morphogenesis [2,3]. For instance, culturing murine adipose stem cell (ASC)-derived intestinal organoids initially in a medium containing epidermal growth factor (EGF), Noggin, R-spondin, CHIR99021 (a glycogen synthase kinase 3-inhibitor), and valproic acid, maintains a high stem population and results in the formation of more uniform and consistent spherical colonies as compared to those cultured in differentiation medium without CHIR99021 and valproic acid [3]. On the other hand, withdrawal of CHIR99021 and valproic acid that regulate Notch and Wnt signaling pathways, results in the differentiation of multiple intestinal cell types, including enterocytes, goblet cells, and Paneth cells while inducing the formation of crypt bud-like structures in the intestine. Organoids, in general, also lack stromal, vascular, and immunological components.

Additionally, the biochemical cues in standard organoid cultures do not correspond to the tissue-specific spatiotemporal signaling and dynamic boundary conditions that are crucial for establishing local signaling gradients and thus for in vivo-like organogenesis [4,135]. The cells and tissues are constantly communicating with each other through various signaling pathways that regulate the development of organs as well as their functions during organogenesis. These signaling pathways are highly specific in determining cell fates, via activating transcriptional programs in response to extracellular signals. Importantly, these signaling pathways undergo changes over time as the organs develop [136]. Furthermore, the biophysical cues, such as fluid flow, shear stress, and mechanical and compressive forces in surrounding microenvironments of developing tissues and organs, play significant roles in directing cellular differentiation and tissue morphogenesis, as well as maintaining the functionality of tissues and organs [137,138]. Therefore, the generation of organoids in standard cultures does not fully replicate the complex process of organogenesis that occurs in vivo. Hence, it is of utmost importance to improve organoid cultures by incorporating the knowledge of organogenesis and comprehending the way cells interact with their surrounding cellular and physical microenvironment within the stem cell niche.

To this end, various strategies have been developed for engineering dynamic boundary conditions, including both cell-intrinsic and cell-extrinsic engineering approaches. In cell-intrinsic engineering, modifications to cell membrane properties or the application of synthetic biology techniques are employed, resulting in programmed cell assembly or controlled gene expression, respectively. On the other hand, cell-extrinsic engineering involves the applications of bioengineering strategies to locally modify the biochemical and biophysical properties of the supporting ECM [139]. Bioengineering approaches, in particular, enable the generation of *in vitro* cell niches that more closely mimic physiological conditions, thereby enhancing organoid culture methods. Additionally, the integration of microfluidic systems contributes in

generating morphogen gradients that can be spatially and temporally adjusted [140]. As such, bioengineering strategies such as 3D bioprinting can be further leveraged that facilitate precise spatial and temporal regulation of differentiation or cell patterning signals during organoid development. 3D bioprinting strategies have emerged as promising approaches for engineering tissues in vitro that typically utilizes computer-aided manufacturing processes to precisely place cells and biomolecules embedded in hydrogel biomaterials in a predefined shape, size, and orientation. 3D-bioprinted constructs provide tissuespecific structures and microenvironments that supply with physiologically relevant cues for tissue maturation and acquisition of biological functions, thus forming complex tissues that closely resemble native tissues or organs [141-143]. Even though the bioprinting approaches have been predominantly used for bioprinting of cells encapsulated in hydrogels, significant advancements have also been made in recent years in the field of 3D bioprinting of organoids. 3D bioprinting of organoids enable precise placement of individual organoids, offering improved control over the arrangement of organoids and overall structures in space while facilitating the direct fusion between organoids resulting in the formation of large-scale functional tissues in vitro [144,145].

In this review, we present the latest advancements in imaging technologies that have been employed in organoid research. In addition, we discuss various bioprinting techniques and biomaterials that are frequently used in the field, with a specific focus on recent progress in organoid bioprinting. The article aims to highlight the rationale underlying the selection of best-matched bioprinting methods and biomaterials that guide the proliferation, differentiation, and morphogenesis while facilitating the multicellular self-organization, leading to the generation of functional engineered tissues across physiologically relevant scales. In conclusion, we recommend selecting appropriate imaging techniques based on the specific requirements of the different studies while summarizing potential strategies and future prospects for organoid bioprinting and imaging.

2. 3D imaging of organoids

Imaging has been crucial in unraveling and understanding the intricate details of organoids. By visualizing the internal structures, cellular organization, and dynamic aspects within organoids, imaging has provided important insights in various fields such as developmental biology, disease modeling, tissue engineering, and regenerative medicine, as well as drug screening [146]. 2D imaging of thin tissue sections after immuno(histo)chemical staining has been used widely to assess internal structures of organoids. This approach enables researchers to observe the distribution pattern of one or more markers within the organoid volumes, thereby providing valuable insights into the structural organizations and functionalities of the organoids [57,147].

While 2D imaging provides important information, it is limited in fully capturing the intricate complexity of 3D structures. Fortunately, recent years have witnessed a remarkable advancement in the field of 3D imaging, introducing revolutionary microscopic techniques capable of examinations across multiple scales, ranging from individual cells to entire tissues. These cutting-edge imaging strategies such as confocal microscopy, two-photon microscopy [148], and light sheet-based microscopy [149] are being successfully implemented in the study of organoids. These techniques enable researchers to obtain highresolution images that reveal the spatial organizations of different cell types, tissue layers, and intricate cellular interactions within the intact organoids. Furthermore, automated 3D live-cell imaging methods enable the continuous observation of growing organoids, facilitating a profound understanding of critical aspects such as cell-fate determination during organogenesis, cellular composition, intercellular interactions, functional characteristics, and dynamic signals within intact living organoids [150-152]. Using an image-based screening platform combined with a chemical genetics approach to study intestinal

organoids can advance our understanding of the mechanisms underlying organoid development and the regenerative capacity of the intestinal epithelium [153]. Here we introduce the most used imaging techniques applied at various spatial scales. Depending on the research objectives and the desired levels of detail, researchers can choose the appropriate imaging technique or employ a combination of different imaging techniques to gain comprehensive insights into the organoids' characteristics (Table 1).

2.1. Electron microscopy

Transmission electron microscopy (TEM) and scanning electron microscopy (SEM) are two widely used techniques for imaging the ultra-structures of various specimens, including organoids [154,155]. TEM involves passing a beam of electrons through a thin specimen, allowing for the visualization of internal structures at very high resolutions. It can provide detailed information regarding cellular components, organelles, and fine structural details. TEM can achieve nanometer-scale resolution, surpassing the capabilities of conventional optical microscopy. However, TEM requires complex sample preparation, including the preparation of ultra-thin sections (nanometer-range) and the imaging process is conducted in a vacuum.

In contrast, SEM scans the surface of the specimen using a focused

beam of electrons. It provides a detailed, 3D representation of the sample's surface topography, allowing for the visualization of surface features and textures [155,156]. SEM offers a larger depth of field compared to TEM, enabling the imaging of samples with uneven surfaces. Sample preparation for SEM is generally simpler than for TEM, and imaging may be performed in a regular atmospheric environment. However, conventional SEM primarily focuses on surface structures and does not provide as much information relating to internal cellular components [155,157].

Thus, both TEM and SEM play important roles in studying organoids. While TEM is well-suited for investigating the internal ultrastructure and finer details of organoid components, SEM offers the advantage of capturing images of samples from various angles, providing insights into their 3D shapes and distributions that are important for studying surface morphologies. For example, TEM images of an airway organoid cross-section exhibited the polarized epithelium comprised of basal, secretory, brush, as well as multi-ciliated cells and apical microvilli (Figure 2A), whereas SEM imaging of an airway organoid showed its 3D surface morphology (Figure 2B) [155].

2.2. Bright-field microscopy

Bright-field microscopy (BFM) is a commonly used technique for

Table 1
Commonly used imaging technologies used for imaging organoids.

Imaging technology	Resolution	Sample preparation	Advantages	Disadvantages	Applications	Refs.
Electron microscopy	~1 nm	Requires fixation, dehydration, and thin sectioning of the sample	High resolution with detailed structural imaging.	Time-consuming preparation; not suitable for live imaging; limited to thin samples; high cost	Ultrastructural studies	[154-157]
Bright-field microscopy	~200 nm (xy); poor axial (z) resolution for large targets	Sample preparation is easy, often using a slide and a cover slip; thin or thick samples	May not need staining; large field of view; high speed; low cost.	Low contrast; low resolution	General cell morphologies; tissue structure	[158-160,162]
Wide-field fluorescence microscopy	~200 nm (xy); poor axial (z) resolution for large targets	Requires fluorescent labeling; thin or thick samples	Easy to use; low cost; large field of view and low phototoxicity; high speed; live cell imaging	Lack of optical sectioning and can image only thin samples	General cell morphologies	[168,170]
Laser-scanning confocal microscopy	~200 nm (xy); ~500 nm (z)	Requires fluorescent labeling	High axial resolution;3D imaging;	Limited depth of penetration; long imaging time; high photobleaching and phototoxicity	Detailed tissue architectures; intracellular structures	[173,174]
Multiphoton microscopy	~200 nm (xy); ~500 nm (z)	Requires fluorescent labeling with limited fluorophores	Deeper penetration depth; less out-of-focus photobleaching	Complex, expensive equipment; long imaging time; phototoxicity with high peak excitation intensity	Deep tissue imaging; dynamic processes in live cells	[177,178,181]
Fluorescence lifetime imaging	~200 nm (xy); poor axial (z) resolution for large targets	Requires fluorescent labeling	Measures fluorescence decay time; provides functional information; less sensitive to photobleaching	Additional signal analysis; expensive setup with photon counting	Biochemical changes; protein interactions	[134,148,182,184]
Light-sheet microscopy	~300 nm (xy); ~600 nm (z)	Requires fluorescent labeling; sample is often semitransparent and embedded in clear gel	High-speed imaging; low photobleaching	Complex setup; limited sample thickness	Long-term imaging of living samples	[187-191]
Super-resolution fluorescence microscopy	~30 nm (xy); ~100 nm (z)	Requires specific fluorescent dyes and sophisticated sample preparation.	Sub-diffraction resolution	may cause serious photobleaching; low imaging speed	Molecular interactions; subcellular structures	[170,204,206,207]
Optical coherence tomography	$\sim\!10~\mu m$ (xy), $<\!10~\mu m$ (z)	Minimal preparation	Non-contact; deep penetration	Low resolution; lack of functional and molecular sensitivity	Tissue morphologies; developmental biology	[210-215]
Photoacoustic tomography	Scalable from a few micrometers to hundreds of micrometers (xy), tens of micrometers to hundreds of micrometers (z)	Minimal preparation; may use contrast agents labeling the molecules.	Deep penetration depth; high optical absorption contrast; inherent depth sectioning; can work with both fluorescent or non- fluorescent samples	Relatively low sensitivity; low imaging speed	Vascular imaging; tissue oxygenation studies	[216-219]

Fig. 2. Electron Microscopy. (A) TEM images of an airway organoid cross-section exhibiting the polarized epithelium comprised of basal, secretory, brush, and multiciliated cells, followed by detailed visualizations of apical microvilli and cilia with their characteristic microtubule structures. Scale bars, $10 \mu m$ (left), $2 \mu m$ (right top), and 500 nm (right bottom). (B) SEM images of a partially opened airway organoid showing its 3D architecture, followed by detailed visualization of apical surfaces of secretory and multi-ciliated cells. Scale bars, $50 \mu m$ (left) and $2 \mu m$ (right). Reproduced under the terms of the Creative Commons Attribution 4.0 International License [155].

imaging organoids, providing a panoramic view that enables the assessment of overall morphology, cellular arrangements, and general structural features of organoids [158,159]. BFM operates on the principle of passing light through the sample, and the resultant image is formed by the differences in light absorption and scattering through the specimen. BFM allows for the observation of organoids under normal, non-specific lighting conditions, making it suitable for routine examinations and qualitative analyses. For example, BFM was utilized to visualize the expansion rates of wild type (WT) and Miller Dieker Syndrome (MDS) patient-derived organoids, which helped in assessing the real-time migration of neuronal cells in both WT and MDS patientderived organoids, starting one day after organoid attachment and continuing for up to 48 h [159]. WT neurons exhibited a characteristic saltatory migration pattern, with an average speed of 20 µm h⁻¹ with track straightness close to 1. In contrast, many of the MDS neurons deviated from saltatory migration and displayed a significantly reduced migration speed of 13 μm h⁻¹ and lower track straightness. BFM produces images by capturing the transmitted light through the specimen, revealing the general structural characteristics and cellar arrangements within the organoids [160]. It is particularly useful for assessing the overall shape and size of organoids, providing vital details about their growth and development. For instance, BFM was used to examine cerebral organoids for size and the presence of ring structures in the peripheral regions of the organoid [161]. Cerebral organoids within the range of 500-700 µm in diameter and having multiple ring structures throughout developed into mature forebrain organoids. Those cerebral organoids lacking ring structures did not successfully mature into organoids. In addition, with extremely low illumination light intensity, BFM is unlikely introduce photobleaching and thus allows for real-time imaging of live organoids, making it suitable for observing dynamic processes or time-lapse studies [162]. BFM has been used to image neuromuscular organoids for studying contraction of skeletal muscle cells through changes based on acetylcholine receptors in the neuromuscular junction [163]. Various deep learning-based tools have been used to localize and quantify human intestinal organoids [164]. These tools can automatically recognize, label, and track individual organoids [165], as well as identify various classes of organoids, including cystic, non-budding, early, late organoids, and spheroids [166].

However, BFM has certain limitations in terms of resolution and the ability to visualize fine details or subcellular structures. The resolution of BFM is generally limited by the wavelength of light and the focusing capability of the optical objective, which restricts its ability to capture nanoscale features. In addition, BFM images are planar, and are not appropriate for 3D imaging. Also, BFM usually does not support fluorescence imaging of the samples. Therefore, if detailed subcellular structural analyses are required, complementary techniques such as fluorescence microscopy and electron microscopy may be more suitable. However, BFM due to its simplicity serves as a valuable tool for initial

observations and characterizations of organoids, complementing other imaging techniques that offer higher resolution, volumetric imaging capacities, and specific information about cellular components [167]. Additionally, BFM is a cost-effective option for routine imaging and does not require specialized equipment.

2.3. Fluorescence microscopy

Fluorescence microscopy is another commonly used imaging technique in the field of biological research, including the study of organoids. It utilizes fluorescent dyes or fluorescently labeled molecules to visualize specific cellular components or molecular processes within the organoids (Figure 3) [168]. In fluorescence microscopy, fluorescent probes are introduced into the sample, targeting specific structures, organelles, or biomolecules of interest. These probes emit fluorescent light with longer wavelengths when excited by a light source. By capturing and detecting the emitted fluorescent light, the microscope creates high-contrast images that highlight the labeled structures or molecules.

One of the major advantages of fluorescence microscopy is its ability to provide specific and localized information. By using different fluorescent probes or markers, various cellular components or molecular events can be visualized simultaneously within the organoids. For example, fluorescence microscopy was used for identifying and characterizing structural features in mammary epithelial organoids, such as the expression of basal cell markers, the presence of multiple lumens per lobule, the edge of mammary structures, and the differentiation and maintenance of luminal cell populations [169]. This allowed for the investigation of various biological processes, such as cell proliferation, apoptosis, protein localization, and gene expression, at the single-cell level [170]. Fluorescence microscopy also offers the possibility of livecell imaging, enabling the observation of dynamic processes and realtime changes occurring within the organoids. This can be achieved through specialized imaging setups that maintain the organoids under controlled physiological conditions [171].

Fluorescence microscopy, despite its advantages, does have certain limitations including use of fluorescent markers or dyes that may sometimes irreversibly alter the imaged samples, rendering them unusable for subsequent analyses or experiments. In addition, fluorescent markers are prone to photobleaching, the gradual fading of fluorescence signal over time, that limits the duration of live-cell imaging experiments and can affect the accuracy and reliability of the acquired data. Furthermore, the excitation light used in fluorescent microscopy can be phototoxic to cells, causing damage or altering their behaviors. Prolonged exposure to intense light can induce cellular stress responses, influence cellular processes, or even result in cell death making long-term, live-cell imaging experiments challenging [172]. Another notable limitation of classical fluorescence microscopy is its inability to

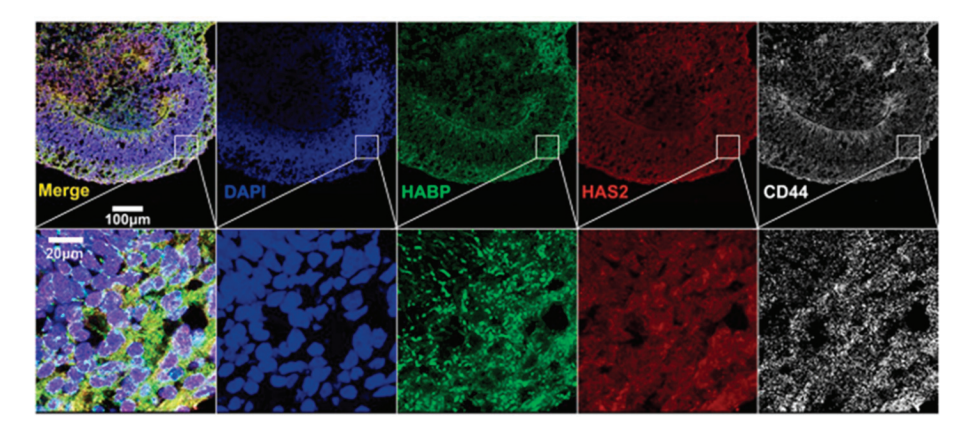


Fig. 3. Fluorescence Microscopy. hiPSC-derived cortical spheroids produced in hyaluronic acid ECM. 10-μm-thick cryosections of 90-day-old control spheroids were stained for ECM component markers, with HA as detected by HABP (green), HAS2 (red), and CD44 (white). Scale bars, 100 μm (top panel) and 20 μm (bottom panel). HA: hyaluronic acid; HABP: hyaluronic acid-binding protein; HAS2: HA synthase; CD44: cluster of differentiation 44 (HA-receptor). Reproduced under the terms of the Creative Commons Attribution 4.0 International License [209].

allow 3D imaging of the samples. While it is effective for imaging monolayer cell cultures and thin tissue sections, its application is limited in the context of 3D samples. This limitation is because the image quality deteriorates as the imaging depth increases, as the fluorophores throughout the entire sample thickness are uniformly excited, resulting in a blurred signal and a strong background.

2.4. Laser-scanning confocal microscopy

Laser-scanning confocal microscopy (LSCM) is a specialized fluorescence microscopy technique and represents a powerful imaging tool used in biological research, including the study of organoids. It uses a laser beam to obtain high-resolution, 3D images of fluorescently labeled samples with improved optical sectioning [173]. In LSCM, a focused laser beam scans the sample point-by-point in a raster pattern. The emitted fluorescent light from the sample is collected by a detector after passing through a pinhole, which eliminates out-of-focus light, resulting in sharper and more precise images. The confocal imaging technique improves contrast and resolution, allowing for better visualization of the labeled structures within the organoids [174].

LSCM offers several advantages for organoid imaging. It enables the capture of optical sections at different depths within the specimen, facilitating the reconstruction of 3D images and providing detailed information about the spatial organization and distribution of cellular components. This is particularly useful for studying complex organoid structures and cellular interactions within the 3D environment. In an example, high-resolution 3D confocal imaging allowed for detailed visualization of the mouse mammary organoid structures, including identification of the cellular composition, observation of cellular morphology and organization, and analysis of luminal organization and functionality [174]. 3D confocal imaging analyses revealed that basalderived organoids possessed K14⁺ and p63⁺ basal cells, along with K8/18⁺ and E-cadherin⁺ luminal cells. Notably, the basal/myoepithelial cells exhibited their characteristic elongated morphology, remarkably resembling the observed morphology in vivo, as they wrapped around buds of cuboidal luminal cells (Figure 4). Additionally, LSCM allows for the visualization of dynamic processes in real-time. Time-lapse imaging with LSCM provides insights into the dynamic behavior and functional changes of organoid systems. For example, LSCM was used to acquire long-term time-lapse imaging of intestinal organoids embedded in triple-decker hydrogel sandwiches comprised of consists of a base coat of poly(2-hydroxyethyl methacrylate), a thin overlay of Matrigel onto which cells were deposited, and a top coat of Matrigel [175]. Similarly, in a recent study, LSCM was used for live imaging of stimulation of OptoShroom3, optogenetic variant of Shroom3 that is a critical regulator of apical constriction in multiple morphogenetic processes in vertebrates, including neural tube closure and lens placode invagination, and the morphogenesis of the gut and kidney [176]. This study demonstrated that an increase in apical tension leads to tissue folding, thickening, flattening, and lumen shrinkage in both epithelial cell sheets and neural organoids.

However, the LSCM imaging process is time-consuming, as the laser scans the sample point-by-point. The high-intensity laser light used in LSCM can also induce photobleaching and phototoxicity, affecting the sample's viability and long-term imaging capabilities. Proper experimental design, including optimizing laser power and exposure time, is essential to minimize these effects [167].

2.5. Multiphoton microscopy

Similar to LSCM, multiphoton microscopy (MPM) also allows for high-resolution, 3D imaging of fluorescently labeled samples using the principle of multiphoton absorption [177,178]. In MPM, instead of using a single high-energy photon for excitation, it utilizes two or more lower-energy photons to excite the fluorophores within the sample simultaneously. This occurs only at the focal point where the photons are most concentrated, resulting in highly localized excitation. The emitted fluorescence is then detected, enabling imaging of specific structures or molecules within the organoids.

The use of multiple photons for excitation in MPM offers several advantages. It reduces the likelihood of out-of-focus photobleaching and phototoxicity compared to traditional confocal microscopy, as the excitation is limited to the focal plane. This enables prolonged imaging sessions, making it suitable for long-term observations of dynamic processes within organoids. For instance, the long-term developmental trend of retinal organoids was monitored by two-photon microscopy, highlighting the shift from predominantly glycolytic phosphorylation to predominantly oxidative phosphorylation between 2 and 3 months of culture [179]. By using longer excitation wavelengths, MPM also provides reduced excitation light attenuation and improved depth penetration compared to traditional microscopy techniques. This allows for imaging deeper into thick samples, such as 3D organoids, while minimizing the background signal and increasing image clarity. In another example, using label-free three-photon imaging, assessment of intact uncleared cerebral organoids could reach up to \sim 2 mm in depth [180]. Moreover, MPM is compatible with a wide range of fluorescent dyes and markers, providing flexibility in labeling specific cellular components or molecules within the organoids. It enables the visualization of various biological processes, such as cell migration, signaling events, and cellular dynamics, with high spatial and temporal resolutions [181].

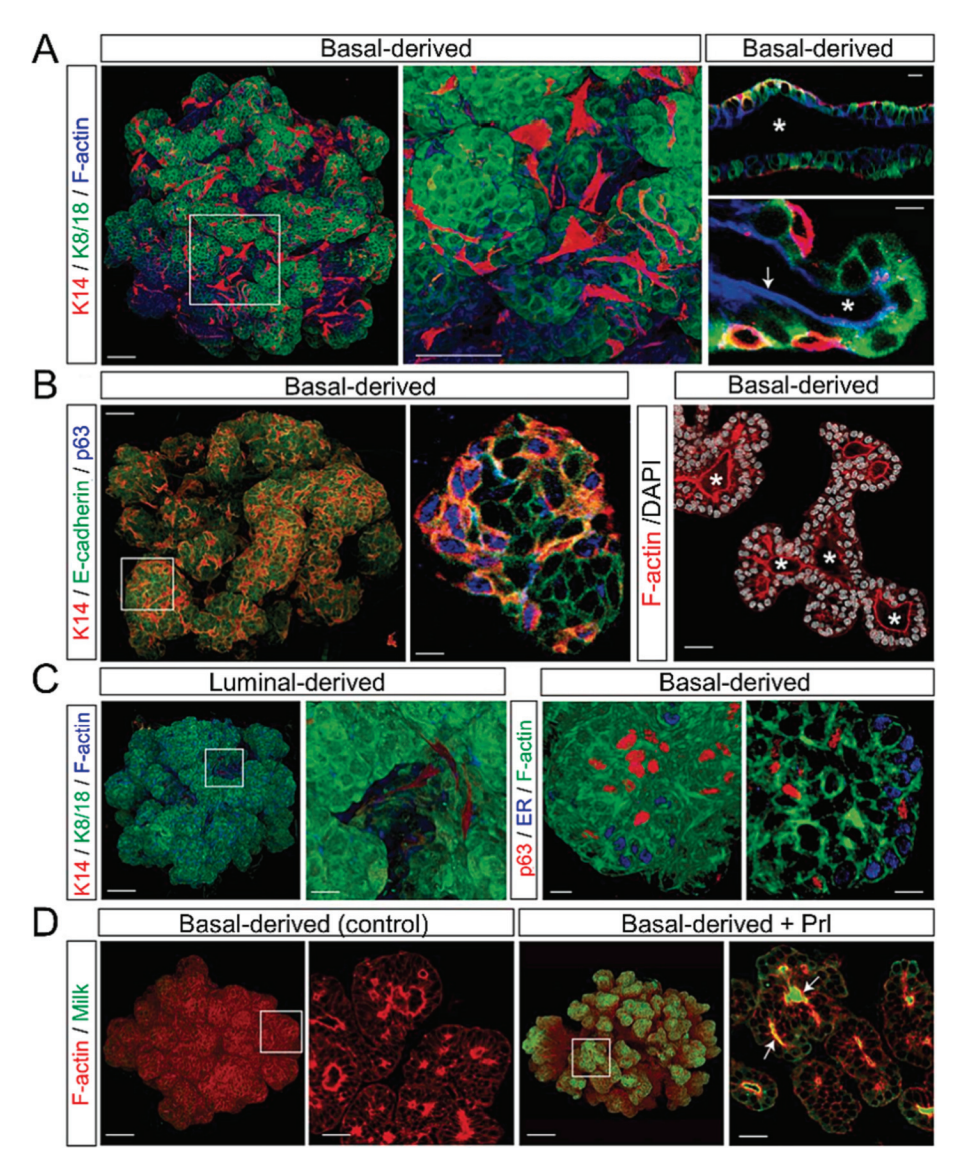


Fig. 4. Laser Scanning Confocal Microscopy. (A) Whole-mount 3D confocal images of basal-derived mammary epithelial organoids, immunostained for K8/18, K14 and F-actin. Scale bars, 25 μm (whole mount) and 5 μm (optical section). (B) Whole-mount 3D confocal image and an optical section of an organoid immunostained for E-cadherin, p63, and K14. Scale bars, 30 μm (whole mount) and 8 μm (optical section). Followed by optical section of an organoid immunostained for F-actin and counterstained for nuclei with DAPI. Scale bar, 20μm. (C) Whole-mount 3D confocal image and an enlarged section of a luminal-derived epithelial organoid immunostained for K8/18, K14, and F-actin. Scale bars: 35 μm (whole mount) and 10 μm (optical section). Followed by a magnified region of a whole-mount 3D confocal image and an optical section of basal-derived organoids immunostained for ER, p63, and F-actin. Scale bars, 8μm. (D) Whole-mount 3D confocal images and magnified optical sections of basal-derived organoids with or without Prl stimulation, immunostained for F-actin and milk. Scale bars, 50 μm (whole mount) and 20 μm (optical section). DAPI: 6-diamidino-2-phenylindole, Prl: Prolactin. Reproduced with permission from The Company of Biologists [174].

However, MPM requires specialized equipment, including a femtosecond pulsed laser as the excitation source. The setup and operation of MPM is more complex and expensive compared to conventional fluorescence microscopy techniques.

2.6. Fluorescence lifetime imaging microscopy

Fluorescence lifetime imaging microscopy (FLIM) measures the fluorescence decay time, or fluorescence lifetime, of fluorophores within a sample to gain crucial insights into molecular interactions, protein dynamics, cellular processes [148], and cell metabolism in organoids [182]. By analyzing the fluorescence lifetime, FLIM can provide quantitative information about the local environment, concentration, and interactions of the fluorophores.

FLIM offers several advantages for organoid imaging. It provides a robust and quantitative measurement of fluorophore behaviors. Unlike

intensity-based imaging techniques, FLIM is less sensitive to factors such as photobleaching and photodamage, making it particularly suitable for long-term, time-lapse imaging experiments for tracking molecular interactions and dynamic processes within organoids. Notably, FLIM can be used for in situ analyses of cancer organoids. For example, it facilitated monitoring of the cellular and metabolic responses to drug treatments such as cisplatin and venetoclax in organoids derived from bladder cancer cell lines, primary tumor biopsy tissue, and patient urine [183]. The non-invasive feature of FLIM enabled monitoring of metabolic changes in these cells, aiding the detection of early adaptive responses to hypoxia. In addition, FLIM can discriminate between different fluorophores with overlapping emission spectra. By analyzing their distinct fluorescence lifetimes, FLIM allows for multiplexing and the simultaneous detection of multiple fluorophores within the organoids. This allows the visualization of multiple molecular components or signaling events within a single experiment, providing fundamental

information regarding complex cellular processes [134,184].

Furthermore, FLIM can be combined with fluorescence resonance energy-transfer (FRET) techniques to study protein-protein interactions and conformational changes within organoids. By measuring changes in fluorescence lifetime resulting from FRET, FLIM-FRET, it enables the investigation of molecular interactions and signaling dynamics in a spatially resolved manner [185]. The integration of FLIM with a custom phasor approach for analyzing FLIM data has been reported for non-invasive detection of shifts in cellular metabolic activities towards glycolysis or oxidative phosphorylation in 3D Caco-2 models of colorectal carcinoma, offering a valuable tool for studying cellular metabolism in 3D cultures [186]. However, FLIM also requires specialized equipment, including a short-pulsed laser, a time-correlated single-photon counting system, and sophisticated data analysis techniques. The setup and operation of FLIM can be more complex compared to traditional fluorescence microscopy techniques.

2.7. Light-sheet microscopy

Light-sheet microscopy (LSM) enables fast, high-resolution imaging of samples while minimizing phototoxicity and preserving sample integrity [187,188]. In LSM, a thin sheet of laser light is used to illuminate a specific plane within the organoid sample. The emitted fluorescence from the illuminated plane is then captured by a separate objective lens positioned perpendicular to the illumination path. This configuration allows for precise optical sectioning, reducing out-of-focus light and providing sharper images with improved contrast and resolution.

LSM offers several advantages for organoid imaging. The use of a light sheet minimizes photodamage to the sample by selectively illuminating only the focal plane of interest. This reduces phototoxicity, allowing for long-term imaging experiments and preserving the viability and functionality of the organoids over extended periods. LSM also allows rapid image acquisition. By illuminating a single plane at a time and capturing the fluorescence from that plane, LSM is able to acquire volumetric data of the entire organoid with high speed and efficiency.

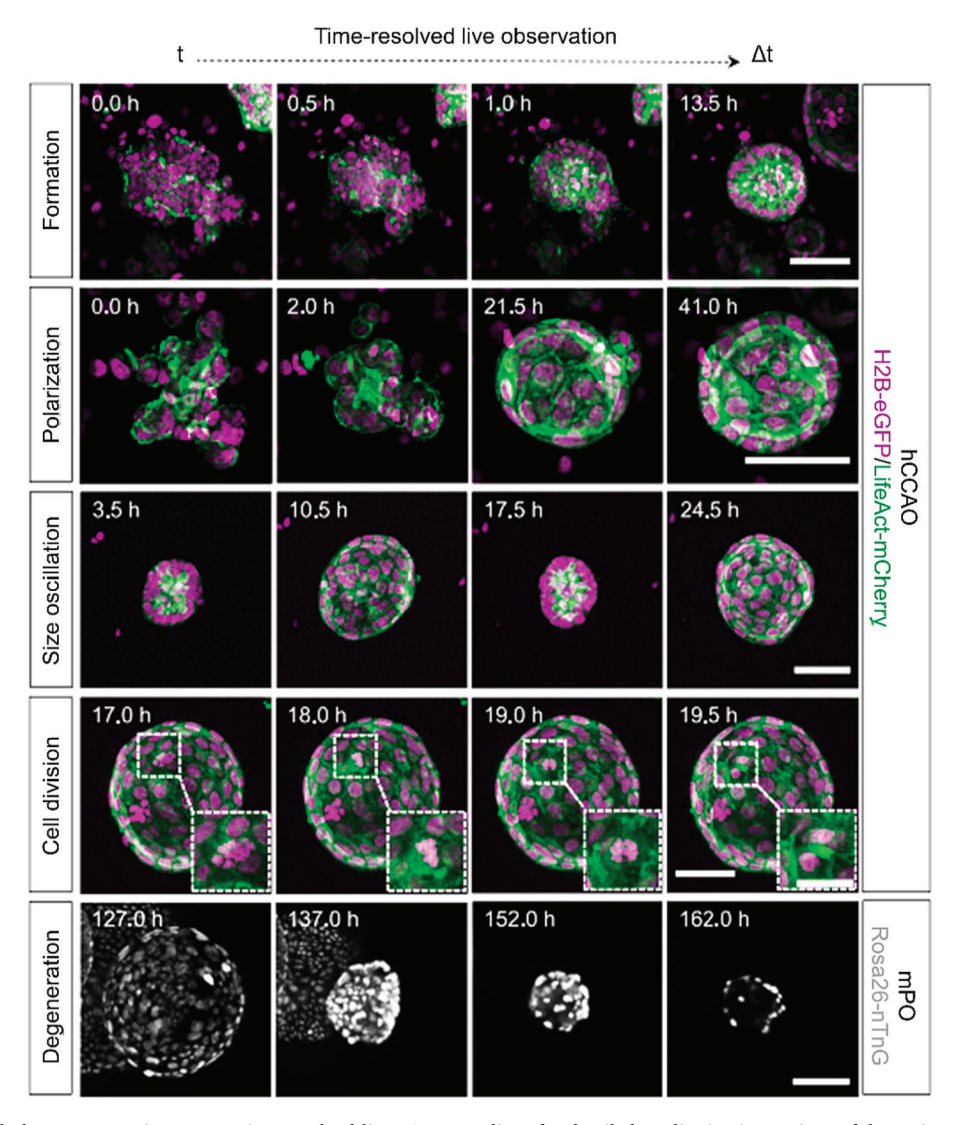


Fig. 5. Light Sheet-based Fluorescence Microscopy. Time-resolved live LSM recordings for detailed qualitative inspections of dynamic morphological processes in organoid development. hCCAOs and mPOs were cultured for long-term live observations. Approximately 120 organoids were recorded in image stacks up to 900 z-planes deep for at most 7 days. The images exhibit maximum intensity z-projections demonstrating the expressions of the nuclei markers, (H2B-eGFP (magenta) or Rosa26-nTnG (grey) and the F-actin cytoskeletal marker, LifeAct-mCherry (green). Scale bars, 50 μm and 25 μm (inset). hCCAOs: human cholangiocarcinoma-derived organoids; mPOs: murine pancreas-derived organoids; H2B-eGFP: histone-enhanced green fluorescent protein. Reproduced under the terms of the Creative Commons Attribution 4.0 International License [194].

This makes it suitable for time-lapse imaging, capturing dynamic cellular processes, and studying the development and behavior of organoids over time [189-191]. Additionally, the optical sectioning capability of LSM provides improved depth penetration, allowing for the imaging of thick, 3D organoid structures, enabling the visualization of intricate cellular arrangements, spatial relationships, and complex interactions within the organoids. However, LSM also requires specialized equipment, including a light-sheet module, high-performance objectives, and precise sample positioning systems. The setup and operation of LSM may be more complex as compared to traditional microscopy techniques.

Furthermore, LSM can also be combined with fluorescence labeling or multi-color imaging, to study specific cellular components or molecular events within the organoids. This flexibility allows researchers to investigate various biological processes, protein localization, and gene expression patterns within the context of organoid systems. Thus, LSM has been used for long-term live imaging with high temporal resolution, such as monitoring the dynamics of the endocrine differentiation in human pancreas organoids for up to 6 days [192]. Light sheet-based fluorescence microscopy was also used to trace the spatial arrangement of clones over 100 hours in developing brain organoids [193] and to observe the morphological changes in pancreas and cholangiocarcinoma organoids up to 7 days (Figure 5) [194].

Various LSM modalities have been developed over the last decade. These include: *i*) lattice LSM, which replaces the conventional Gaussian beam with the Bessel beam [195], and overcomes the light diffraction of conventional LSM and enabled high temporal and spatial resolution [149,196]; *ii*) dual-sided illumination LSM, which eliminates light scatter seen at the far end of single illuminated objects, enabling imaging the larger target [197], and is applicable for imaging organoids, both live or fixed specimens [194,198-200]; and *iii*) inverted LSM, that requires a V-shaped sample holder to benefit the sample mounting and medium exchange for long-term imaging [192,193,200-203].

Recently, a unified light-sheet imaging framework, LSTree, was introduced that converts extended light-sheet imaging of live intestinal organoids into digital representations known as 'digital organoids' [191]. Utilizing deep learning techniques, the framework accurately segmented individual organoids, including their lumens, cells, and nuclei in 3D over extended time intervals. Simultaneously, large lineage trees were predicted for each organoid and adjusted to iteratively enhance the tracking and segmentation performances over time. The framework was found to effectively segment and track the growth of intestinal organoids from single cells for several days, encompassing biological scales until the organoid reaches a size of hundreds of cells. Information on organoid, lumen, cell, and nucleus volumes, along with other multivariate features, can be visualized simultaneously with lineage tree data which were further analyzable using a web-based Digital Organoid Viewer, facilitating a comprehensive understanding of dynamics at subcellular resolution.

2.8. Super-resolution fluorescence microscopy

Super-resolution fluorescence microscopy (SRFM) is an advanced imaging technique that surpasses the diffraction limit of traditional fluorescence microscopy, allowing for the visualization of fine cellular details and molecular structures within organoids at a higher resolution [170]. In SRFM, several innovative approaches are used to overcome the diffraction limit, which traditionally restricts the resolution of optical microscopy to around half the wavelength of light used. By adopting specialized imaging techniques, SRFM achieves resolution enhancements, enabling the observation of subcellular structures and molecular interactions with greater clarity.

One commonly used SRFM technique is stimulated emission depletion (STED) microscopy. In STED microscopy, a focused gaussianshaped laser beam is used to excite the fluorophores in the sample, while a second, doughnut-shaped laser beam is applied to deplete the fluorescence from the outer regions. By carefully controlling the intensity and timing of the depletion beam, STED microscopy can effectively shrink the point spread function, allowing for super-resolution imaging [204]. For example, dual-color gated STED imaging could obtain a pixel size of approximately 80 nm when imaging microglial in cerebral organoids [205]. However, the main drawback of STED microscopy is that high laser intensity can cause severe photobleaching and phototoxicity [206].

Another approach in SRFM is stochastic optical reconstruction microscopy (STORM). STORM utilizes the controlled activation and stochastic blinking of individual fluorescent molecules to capture their precise positions. By repeatedly imaging and localizing these molecules, a super-resolution image is reconstructed, providing detailed information about the spatial organization and distribution of labeled structures within the organoids. STORM can achieve nanometer-scale lateral and axial resolutions [207]. Nevertheless, there are mainly three limitations of STORM. First, the temporal resolution of STORM is low. Second, STORM imaging relies on blinking fluorophores, and fluorophores' quality and sample preparation are essential. Third, STORM can only image thin samples of no more than a few micrometer-scale since the thick tissues will involve strong scattering [208]. STORM has been used to acquire images of cortical spheroids that enabled detection of distinct pre- and post-synaptic compartments within 3D cortical spheroids (Figure 6) [209]. SRFM also requires specialized equipment, including high-performance lasers, sensitive detectors, and sophisticated image reconstruction algorithms. The setup and operation of SRFM can be complex, and data analysis may involve post-processing techniques to generate super-resolution images.

2.9. Optical coherence tomography

Optical coherence tomography (OCT) is a laser interferometry-based imaging technique that provides a non-invasive, high-resolution imaging of translucent or opaque biological tissues with excellent depth penetration, allowing for the visualization of internal structures and morphological features [210,211]. In OCT, a low-coherence light source, typically a near-infrared laser, is used to illuminate the sample. The backscattered light from the sample is interfered with a reference beam, and the resultant interference pattern is measured. By analyzing the interference pattern, OCT generates cross-sectional images of the sample, similar to ultrasound imaging but with higher resolution.

OCT provides high-resolution, real-time imaging with micrometerscale axial and lateral resolutions. This allows for the visualization of fine tissue structures, cellular arrangements, and organoid morphology in a label-free manner, providing important insights into the development, organization, and functionality of organoids [212]. Additionally, OCT is a non-destructive imaging technique and has good depth penetration capability, enabling imaging of organoids over time while preserving their integrity and behaviors, thus contributing to the understanding of the complex 3D architecture, layering, and cellular interactions within the organoids [213-215]. This method is particularly useful for long-term studies, enabling continuous monitoring of organoid development and behavior while minimizing damage to the tissues. OCT's depth penetration capabilities also make it ideal for examining complex 3D structures within organoids. The disadvantage of OCT is that when the laser penetrates through the sample, it will produce a distant shadow, which is not suitable for observing internal structures of strongly-scattering samples [212]. In addition, it also requires specialized equipment, including high-performance light sources, interferometers, and sensitive detectors. The setup and operation of OCT systems may involve specific sample preparation procedures and image processing techniques for data analysis and visualization [212]. Moreover, OCT usually lacks the molecular sensitivity to different cell types or molecular activities.

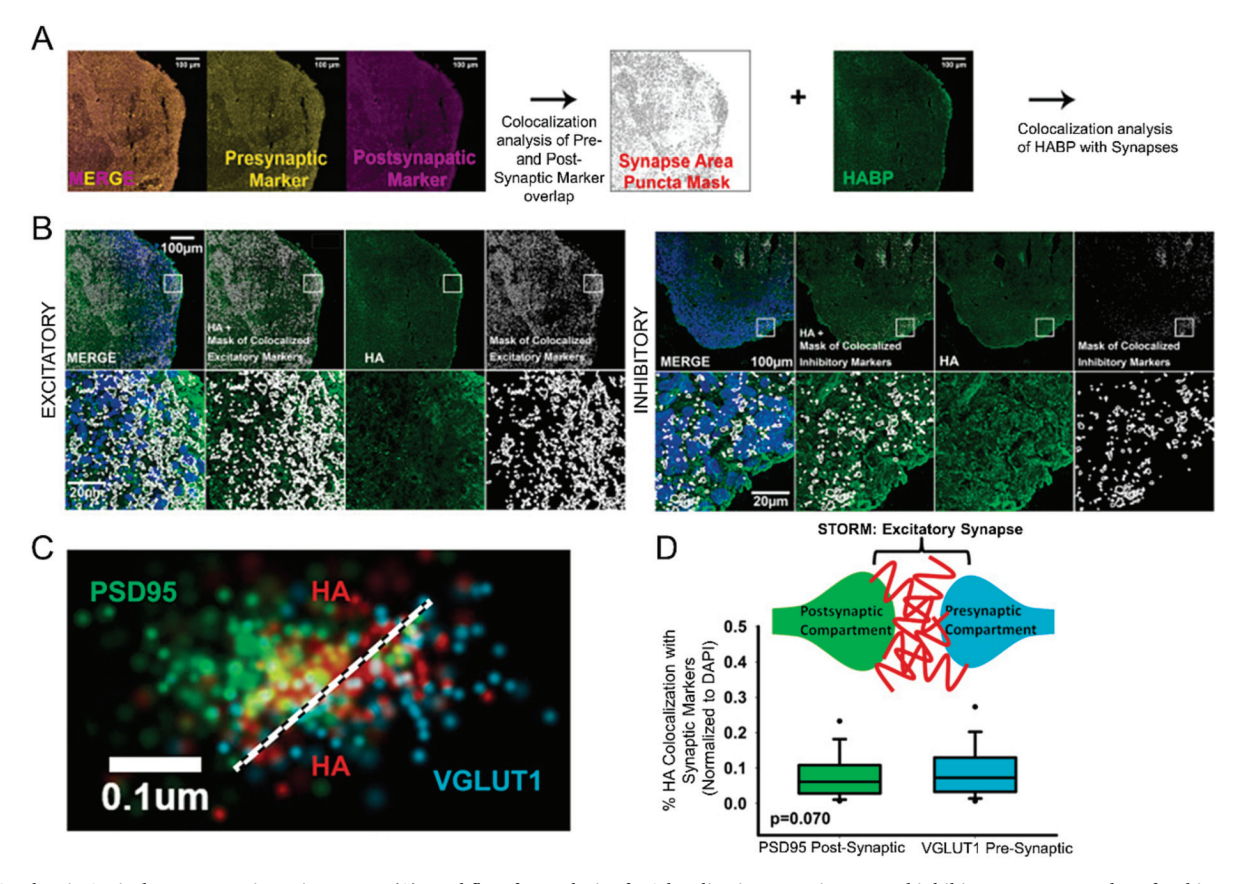


Fig. 6. Stochastic Optical Reconstruction Microscopy. (A) Workflow for analysis of HA localization at excitatory and inhibitory synapses and confocal images of preand post-synaptic markers to identify colocalization in synapses and HA. Scale bars, 100 μm. (B) Images showing the expression of excitatory synapse markers, vGlut-1 and PSD-95, and inhibitory synapse markers, vGAT and gephyrin, along with DAPI (blue) and HA (green). Identified synapses are indicated by white outlines. Scale bars, 100 μm. (C) STORM imaging to visualize HA (red), pre-synaptic marker (vGlut-1, blue), and post-synaptic marker (PSD-95, green) at individual excitatory synapses. It should be noted that HA is positioned between the pre- and post-synaptic compartments of the excitatory synapse. (D) Quantification of the distance between HA and the pre-synaptic marker, vGlut-1, and post-synaptic marker, PSD-95, as determined by measuring the displacement of the maximum peak intensities. HA: hyaluronic acid; vGlut-1: vesicular glutamate-transporter 1; PSD-95: postsynaptic density protein 95; vGAT: vesicular GABA-transporter. Reproduced under the terms of the Creative Commons Attribution 4.0 International License [209].

2.10. Photoacoustic tomography

Photoacoustic tomography (PAT) is an emerging imaging technique that combines the principles of optical excitation and laser-induced photoacoustic effect to visualize biological tissues, including organoids, with high resolution and contrast [216,217]. PAT provides deep imaging by utilizing the photoacoustic effect, where pulsed laser light is absorbed by tissues, resulting in the generation of ultrasound waves that are detected and used to reconstruct images. In PAT, a short-pulsed laser beam is directed towards the organoid sample, causing localized heating and expansion. This leads to the generation of ultrasound waves, which are detected by ultrasound transducers. The detected ultrasound signals are then processed to create a 3D image of the organoid.

PAT presents several advantages for organoid imaging. It provides excellent spatial resolution at depths that are typically inaccessible to other imaging modalities. By combining the high-resolution capabilities of ultrasound with the optical absorption contrast of photoacoustic signals, PAT enables the visualization of cellular structures and fine details within the organoids. PAT is a label-free imaging technique that eliminates the need for exogenous contrast agents or dyes and allows for non-invasive imaging of organoids while preserving their integrity and functionality. Furthermore, PAT can provide functional information by exploiting different optical wavelengths. By selecting specific laser wavelengths, PAT is able to measure the absorption spectra of different tissue components, allowing for the characterization of specific molecules or functional parameters within the organoids [218]. PAT may also

be combined with other imaging modalities, such as fluorescence or ultrasound imaging, to provide complementary information regarding the organoids' structures and functions [218,219]. This multimodal imaging approach enhances the understanding of organoid biology and facilitates comprehensive studies [220]. Nevertheless, PAT also requires specialized equipment, including pulsed laser sources, ultrasound transducers, and sophisticated image-reconstruction algorithms. PAT often requires acoustic coupling medium such as water or ultrasound gel, which might not be applicable to some organoid studies. The setup and operation of PAT systems may involve careful optimization of laser parameters and imaging protocols for optimal results.

2.11. Other imaging modalities

Besides the abovementioned commonly used imaging modalities, some other imaging modalities have also been used for organoids with specific imaging requirements. For example, swept confocally aligned planar excitation microscopy (SCAPEM), a hybrid imaging technique that combines elements of both LSCM and LSM, uses a single objective for both illumination and detection purposes. Such an arrangement allows SCAPEM to image conventional imaging slides and plates, making it compatible with standard microscopy setups, facilitating high-throughput imaging, as it eliminates the need for specialized sample chambers or preparation techniques associated with LSM [221]. Similarly, Brillouin microscopy, in conjunction with LSCM, utilizes a laser to interact with heat-induced pressure waves within a sample, enabling the

measurement of the scattering spectrum. This imaging technique allows for high spatial resolution imaging while also providing information about the mechanical properties such as viscoelasticity of the sample [222]. Likewise, in recent years Raman microspectroscopy (RM) has demonstrated its advantages in imaging organoids. The combination of Raman microscopy with the chemical analysis technique, Raman spectroscopy, has demonstrated its potential as analytical tool for both quantitative and qualitative assessments of biological samples at the molecular level [223]. RM facilitates a detailed analysis of the molecular composition and changes within organoids without altering their natural states, showcasing its ability for non-invasive, label-free, and highly specific chemical characterizations at a microscopic level [224]. For instance, RM was employed for assessing the metabolic states of brain organoids, providing insights into neurodevelopmental disorders [225]. Additionally, it has been applied to evaluating the maturation and functionality of kidney organoids, contributing to the understanding of kidney development and diseases [226]. Moreover, expansion microscopy (ExM) that physically expands the samples has emerged as an innovative imaging tool for organoid imaging [227]. It allows for highresolution imaging over large volumes and significantly improves quality of labeling, clarity of images, and accuracy of subsequent image analyses compared to standard chemical immersion clearing methods. Related, phototransfer by allyl sulfide exchange-ExM (PhASE-ExM) has shown the potential to achieve in situ super-resolution imaging of organoids and ECM interactions [228]. Some other technologies also hold the potential for unraveling profound insights into cell dynamics and interactions within their native microenvironments in organoids. For example, Image-seq, combined with high-resolution imaging with single-cell RNA sequencing allowed for the isolation of cells from specific spatial locations under image guidance while preserving their spatial context [229]. A comprehensive study of the development of human retinal organoids has been achieved by combining iterative indirect immunofluorescence imaging, single-cell transcriptome, and chromatin accessibility analysis [230].

In addition to abovementioned imaging modalities, diffuse optical imaging methods, such as diffuse optical tomography and diffuse correlation spectroscopy have been developed to image strongly scattering samples, with significant compromise in the spatial resolution [231]. Structured illumination microscopy, combined with two-photon excitation, was also shown to improve the depth penetration of superresolution imaging in thick scattering samples [232,233].

Furthermore, overcoming the challenges of 3D imaging posed by the light scattering can be achieved through the utilization of optical tissue clearing (OTC) methods [131,234,235]. OTC methods, such as Benzoic Acid Benzyl Benzoate (BABB) [236], Three-dimensional Imaging Solvent-Cleared Organs (DISCO) [237,238], Clear, Unobstructed Brain/ Body Imaging Cocktails and Computational analysis (CUBIC) [239], See Deep Brain (SeeDB) and Clear Lipid-exchanged Acrylamide-hybridized Rigid Imaging/Immunostaining/in situ-hybridization-compatible Tissue hYdrogel (CLARITY) [240] and fructose, urea, and glycerol (FUnGI3) [132], reduce the scattering of light by homogenizing the refractive index of tissues, enabling clear observation throughout the sample thickness [131]. Of note, ExM can simultaneously achieve sample-clearing while expands it [227]. Various non-invasive opticalsectioning microscopic technologies, including confocal, SRFM, MPM and LSM, have been combined with OTC methods that enabled the acquisition of images of whole 3D organoids, facilitating the study of structural complexity, spatial distribution pattern, phenotypic identity, and cellular states of all individual cells constituting the 3D human cellderived organoids [131,234]. For examples, OTC using FUnGI3 facilitated the acquisition of human airway organoid immunolabeled with acetylated-tubulin using SRFM and human colonic organoid labeled for F-actin using MPM and LSM [131,132]. Thus, the diverse imaging methods can be leveraged together with OCT methods to efficiently address the challenges associated with imaging strongly scattering organoids.

3. 3D bioprinting

3D bioprinting, a form of additive biomanufacturing technology, has been widely used in tissue engineering and regenerative medicine due to its remarkable capacity to control the deposition of cells, hydrogel biomaterials, and/or biologically active molecules precisely in a predefined planar or 3D architecture to produce functional tissues or organs [143,241,242]. Typically, the bioprinting procedure entails several stages, starting with the imaging of the target tissue using medical imaging techniques. This is followed by the utilization of computer-aided design/computer-aided manufacturing software to create a blueprint of the tissue's structure. The next steps involve preparing the bioink by combining appropriate cells or/and biomaterials, bioprinting of the tissue, and culturing and maturing the tissue in vitro [243]. 3D bioprinting can be broadly categorized into extrusion-based bioprinting [244-246], inkjet-based bioprinting [247-249], light-assisted bioprinting [250-256], and other bioprinting approaches such as laserassisted bioprinting [257,258] and Kenzan bioprinting [259,260], among others. Each bioprinting method has unique advantages and disadvantages, and they vary in multiple aspects including the type of bioinks used, bioprinting resolution (Table 2) and thus the intricacy of bioprinted structure produced [261].

3.1. Extrusion-based bioprinting

Extrusion-based bioprinting involves loading hydrogel-based bioinks into a printhead and extruding them from a nozzle to generate filaments that are then deposited in a layer-by-layer manner to construct the desired structures [244,245,262,263]. There are two subcategories of extrusion-based bioprinting techniques, namely pneumatic extrusion and mechanical extrusion. Pneumatic extrusion utilizes compressed air to extrude bioink from a nozzle (Figure 7A) whereas mechanical extrusion utilizes either a piston (Figure 7B) or a screw (Figure 7C) to apply mechanical force to extrude the bioink. Extrusion-based bioprinting has been utilized to create 3D tissue structures with high cell densities by bioprinting bioinks containing cells or even only cells in the form of single-cell suspension or cell spheroids [244,264]. The versatility of extrusion-based bioprinting in depositing a variety of biocompatible bioink formulations, such as cell pellets, organoids or spheroids, and hydrogels including decellularized ECM (dECM), makes it arguably the most commonly used bioprinting approach [264]. In addition, this bioprinting method offers both cost-effectiveness and ease of use as compared to other bioprinting techniques such as inkjet- and light-based bioprinting methods [244,245].

Over time, various adaptations of extrusion-based bioprinting have been developed including co-axial bioprinting, embedded bioprinting, and chaotic bioprinting. Co-axial bioprinting enables biofabrication of standalone solid or hollow tubular fibers by simultaneous extrusion of two or more hydrogel bioink components including oftentimes alginate in addition to those based on gelatin or collagen, among others, with or sometimes without cells, and a crosslinker solution through a coaxial nozzle made up of two or more concentric needles [246,265-267]. The biofabrication of hollow tubular fibers involves dispensing of a singlelayer or multilayer hydrogel sheath and a core of calcium chloride (CaCl₂) for instant physical crosslinking of the hydrogel (Figure 7D). This method is commonly used for biofabrication of functional cannular tissue structures such as vascular, intestinal, and ureteral tissues [265-269]. On the other hand, the extrusion of hydrogel bioink through a core and a crosslinker solution through the outer needle of the co-axial nozzle results on the formation of solid fibers (Figure 7E). Depending on the bioinks used, these bioprinted tubular fibers can be further chemically stabilized by using additional crosslinking methods, such as photocrosslinking [266] and enzymatic crosslinking [265]. This method is generally used for biofabrication of functional osteochondral and cartilage tissues [270-272]. It is possible to generate fibers with tunable dimensions by adjusting the flow rates of one or more hydrogel bioinks

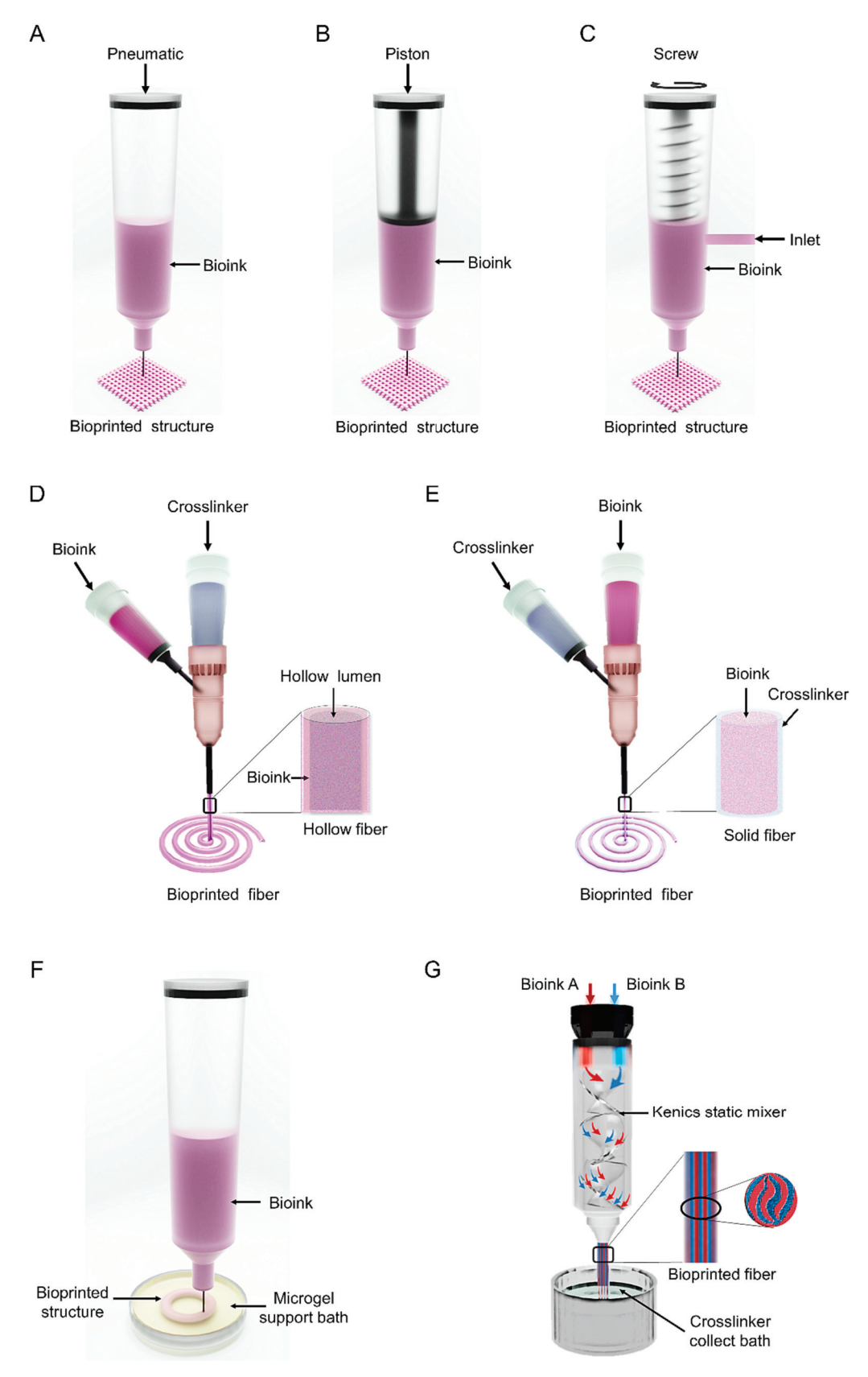
Table 2Common 3D bioprinting modalities and their general characteristics (may subject to changes with specific bioprinting systems).

3D bioprinting modality	Description	Resolution range	Advantages	Disadvantages	Applications	Refs.
Conventional extrusion bioprinting	Compressed air or mechanical screw or piston drives the bioink through a nozzle	100–2000 μm	Multi-material bioprinting; high scalability; high cell density; cost-	Nozzle clogging; moderate cell viability due to shear stress	To biofabricate 3D tissue structures in a layer-by-layer manner	[244,245,262-264]
Co-axial extrusion bioprinting	Simultaneous extrusion of bioinks and crosslinker solution through coaxial nozzle	200—2000 μm	effective	Complex setup; challenges in tuning flow rates for each bioink simultaneously	To biofabricate standalone solid or hollow tubular fibers	[246,265-269]
Embedded extrusion bioprinting	Extrusion of bioink into supportive bath into a support bath that holds the bioprinted structure.	∼20 µm		Challenges in removal of support matrix; may require additional processing steps	To biofabricate complex tissue structures using mechanically weak bioinks	[246,273-276,280]
Chaotic extrusion bioprinting	Chaotic flow of two or more bioinks using a nozzle equipped with a Kenics static mixer	~10 µm		Nozzle clogging; moderate cell viability due to shear stress; not suitable for high- viscosity bioinks	To generate continuous fibers with internally aligned lamellar microstructures	[291,292,297-299]
Inkjet-based bioprinting	Electrically heated printhead or piezoelectric actuator ejects small droplets of bioink out of the nozzle	∼50 µm	High bioprinting speed; precise deposition of bioink droplets; cost- effective	Low cell viability; non- uniform droplets; printhead clogging; requires low cell density and low viscosity bioinks	To biofabricate tissue scaffolds by precise placement of small droplets of bioink onto a substrate	[247,300- 302,305,308,310- 312]
Stereolithography	Either single- or two- photon laser and raster scanning selectively that cures a bioink in a point- by-point manner	∼1 µm	Nozzle-free; relatively fast bioprinting speed; high cell viability	Requires photocurable bioinks; moderate cost	To biofabricate tissue structures by exposing bioink to the laser that selectively cures a bioink in a point-by-point manner	[313-316]
Digital light processing	Either UV or visible light prepatterned from a projector selectively that cures the bioink in a layer-by-layer manner	~35—100 µm			To biofabricate tissue structures by exposing light through a digital mask or pattern onto the surface of the bioink in a layer-by- layer manner	[253,314,325,326]
Volumetric bioprinting	Simultaneous exposure of UV or visible light onto a rotating vat of bioink that creates a desired structure in a single step	~40—100 μm			To biofabricate geometrically complex tissue construct in a centimeter-scale in a single step.	[250,332-335]
Laser-assisted bioprinting	Precise deposition of the bioink onto a substrate using laser pulses	~10 — 100 µm	High precision; relatively fast bioprinting speed; high cell density	Limited cell viability; requires high-viscosity bioinks; comparatively high cost	To facilitate tissue regeneration <i>via</i> bioprinting using single cells or cell aggregates	[255,341,347,348]
Kenzan bioprinting	Precise positioning of spheroids within a microneedle array to fused into tissue constructs	Spheroids of ~500 µm in diameter are fused to form larger tissue constructs	High cell density; high cell viability; may not require supporting biomaterial scaffold	Requires pre-fabrication of spheroids; complex bioprinting setup; may induce damage due to needle	To biofabricate tissue structures utilizing cell spheroids as the fundamental building blocks	[259,351,352]

and the crosslinker solution such as CaCl₂.

Embedded bioprinting enables the biofabrication of complex tissue structures by extruding bioinks into a support bath that holds the bioprinted structure in place until it is cured (Figure 7F) [246,273-275]. This approach is particularly useful for bioprinting complex tissue structures using mechanically weak hydrogels such collagen [276], tropoelastin [277,278], Matrigel [279], and dECM [280]. Other extrusion-based bioprinting methods face difficulties with these hydrogels due to low viscosity, gravity-induced collapse, and deformation of the bioprinted structures. In addition to supporting the bioprinted structure, the support bath also provides an environment during the bioprinting process that maintains high cell viability. Gelatin [12], alginate [281], agarose [282], hyaluronic acid (HA) [283], xanthan gum [281], and gellan gum [284] have been commonly used as supporting matrices, in the form of bulk hydrogels [276,285], granular hydrogels or microgels [276,286], and hydrogel microparticle composites [287,288]. Embedded bioprinting has demonstrated its effectiveness in biofabricating vascular-like networks [285,289] and other complex tissue constructs including heart with internal structures [290].

Chaotic bioprinting involves chaotic flows generated by a printhead equipped with a Kenics static mixer (KSM) featuring multiple mixing elements and two or more inlets (Figure 7G) [291,292]. It is used to generate continuous fibers with internally aligned lamellar microstructures through the repeated action of reorienting and splitting the bioinks, such as alginate, as they travel along the mixing elements. The bioprinted fiber is typically crosslinked using CaCl2 at the KSM exit to achieve stabilization. KSM enhances mixing of two or more bioinks under laminar flow conditions, causing split of each bioink at the forefront of each mixing element and takes the shape of the patterns created by that element. As the bioink moves through each subsequent mixing element, the patterns continue to divide resulting in an increasing level of layering. To be precise, the number of layers produced is 2ⁿ, where 'n' represents the number of elements in the KSM [293-296]. Thus, chaotic bioprinting produces fibers with high precision, speed, and predictability and is particularly useful for producing complex and heterogeneous tissue structures that possess interfaces and striations, like those found in muscle tissues [297-299].



(caption on next page)

Fig. 7. Extrusion-based bioprinting methods. (A) Pneumatic pressure-driven extrusion bioprinting and mechanical force-driven extrusion bioprinting using (B) piston or (C) screw. In pneumatic extrusion bioprinting, air pressure provides the driving force whereas in mechanical extrusion bioprinting, direct piston-driven or screw rotation-driven force causes mechanical displacement, thereby enabling continuous flow of bioink through the nozzle. (D) Co-axial bioprinting of hollow tubular fiber by simultaneous extrusion of hydrogel sheath and a core crosslinker solution. (E) Co-axial bioprinting of solid fiber by simultaneous extrusion of hydrogel bioink through a core and a crosslinker solution through the outer layer. (F) Embedded bioprinting of a ring structure within the support bath. The support bath is responsible for securing the bioprinted structure in position until it undergoes the curing process. (G) Continuous chaotic bioprinting of fibers with internally aligned lamellar microstructures. Chaotic bioprinting uses KSM possessing multiple mixing elements that facilitates the mixing and splitting of two or more bioinks under laminar flow conditions.

3.2. Inkjet-based bioprinting

Inkjet-based bioprinting allows for the precise placement of small droplets of bioink onto a substrate in a precise pattern to create 3D tissue structures [300-302]. There are two methods for generating droplets in inkjet-based bioprinting, *i.e.*, thermal and piezoelectric methods (Figure 8). The thermal method uses electrically heated printhead to vaporize a small amount of bioink and create a bubble that pushes a droplet out of the nozzle (Figure 8A) [303,304]. The piezoelectric method, on the other hand, uses a piezoelectric actuator to generate acoustic waves that form bioink droplets at regular intervals (Figure 8B) [305]. Hydrogel bioinks that are frequently used for inkjet-based bioprinting include alginate [248], chitosan [306], collagen [304], silk [307], and poly(ethylene glycol) [308].

In general, inkjet bioprinting offers the advantages of high speed, high resolution, and low costs, making it well-suited for bioprinting complex structures with fine details. However, inkjet-based bioprinting has some limitations. This technique is constrained by the potential cell death due to high temperature and mechanical stress generated locally when droplets are ejected from the printhead [309]. Another limitation is the formation of non-uniform droplets by inkjet printhead, which can impact the accuracy and reproducibility of the bioprinted structures. Furthermore, printhead clogging is an additional constraint associated with inkjet-based bioprinting due to the high viscosity of the bioink or the presence of cell aggregates or debris in the bioink. Several studies

have been done to investigate the potential of inkjet-based bioprinting in tissue engineering and tissue regeneration, including but not limited to cardiac tissues [310], vascular tissues [247,311], bone [308], as well as *in situ* cartilage repair [312].

3.3. Light-assisted vat-polymerization bioprinting

Light-assisted vat-polymerization bioprinting is a nozzle-free bioprinting method that uses a vat to hold photocurable bioink and a light source, mostly ultraviolet (UV) or visible light, that triggers photopolymerization of bioink, in the presence of photoinitiator, to create 3D tissue structures [313-315]. A photoinitiator is a chemical compound that initiates or triggers a chemical reaction upon exposure to light [316]. When a photoinitiator is subjected to specific wavelengths of light, it undergoes a photochemical reaction that generates highly reactive free radicals or cations. These reactive species then initiate a chain or cationic polymerization reaction, leading to the crosslinking and solidification of the bioink. The commonly used UV/blue-light photoinitiators include 1-[4-(2-hydroxyethoxy)-phenyl]-2-hydroxy-2methyl-1-propane-1-one (Irgacure 2959) and lithium phenyl-2,4,6trimethylbenzoylphosphinate (LAP) [317]. On the other hand, common visible-light photoinitiators include eosin Y [318,319] and tris(2,2bipyridyl)dichloro-ruthenium(II) hexahydrate/sodium persulfate (Ru/ SPS) [251,320].

Light-assisted bioprinting often incorporates biocompatible

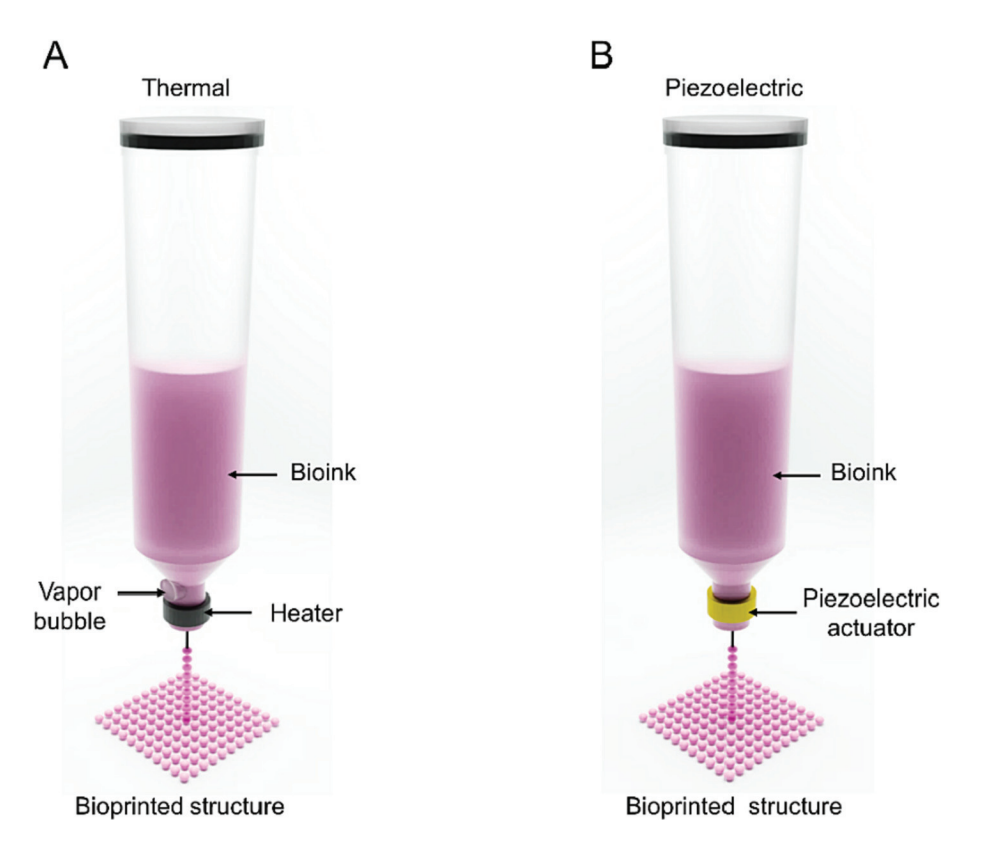


Fig. 8. Inkjet-based bioprinting methods. Thermal inkjet-based bioprinting that uses (A) electrically heated printhead to create bioink droplets and (B) piezo-electric inkjet-based bioprinting that uses a piezoelectric actuator to generate bioink droplets.

photoabsorbers along with photoinitiators in the bioink formulations. Photoabsorbers are dyes absorbing and attenuating light by competing with the photoinitiator for photons [316]. As such, the inclusion of a photoabsorber in the bioink formulation helps prevent over-curing of the bioink and improve the printability of internal structures. Nevertheless, the presence of a photoabsorber causes an exponential decay in light intensity that results in a gradual change in curing levels within each bioprinted layer, leading to variations in the mechanical properties of the bioprinted structure. Commonly used photoabsorbers for bioprinting applications include soluble natural or synthetic food dyes such as tartrazine [321], anthocyanin [321], Ponceau 4R [322], 2-hydroxy-4methoxybenzophenone-5-sulfonic acid [323], due to their biocompatibility and low toxicity. The selection of photoinitiators and photoabsorbers depends on several factors such as the desired curing mechanism, the wavelength of light used for curing, and the compatibility with the bioink formulations. These factors have a direct impact on the properties of the bioink, the speed of curing, the mechanical characteristics, the resolution, and the overall quality of the bioprinted structures. Consequently, selecting the appropriate photoinitiators and photoabsorbers is crucial to achieve the desired bioprinting outcomes [316,321,324]. The widely used or emerging light-assisted bioprinting methods include stereolithography (SLA), digital light processing (DLP), and volumetric bioprinting [315]. Each of these methods utilizes light in a distinct way to facilitate the bioprinting process and achieve desired outcomes.

SLA utilizes either single-photon lasers (single-photon laser lithography) or two-photon lasers (two-photon laser lithography, also known as multiphoton polymerization lithography) and raster scanning to selectively cure a bioink in a point-by-point manner. In a typical bottom-up configuration, the light source selectively cures the bioink, following the path generated by sliced 3D computer-aided design model, to form a thin solid layer. Following the formation of the pattern for each layer, the build platform is gradually lifted out of the vat while the bioink is exposed to a light source. During this lifting process, each layer of the structure is built, with the build platform being lifted by a small distance between each layer. Once the building process is complete, the uncured bioink is drained from the vat and then the 3D-bioprinted structure is removed (Figure 9A). SLA bioprinting offers high resolutions and fast bioprinting speeds, but it has limitations related to scalability and post-processing requirements [314].

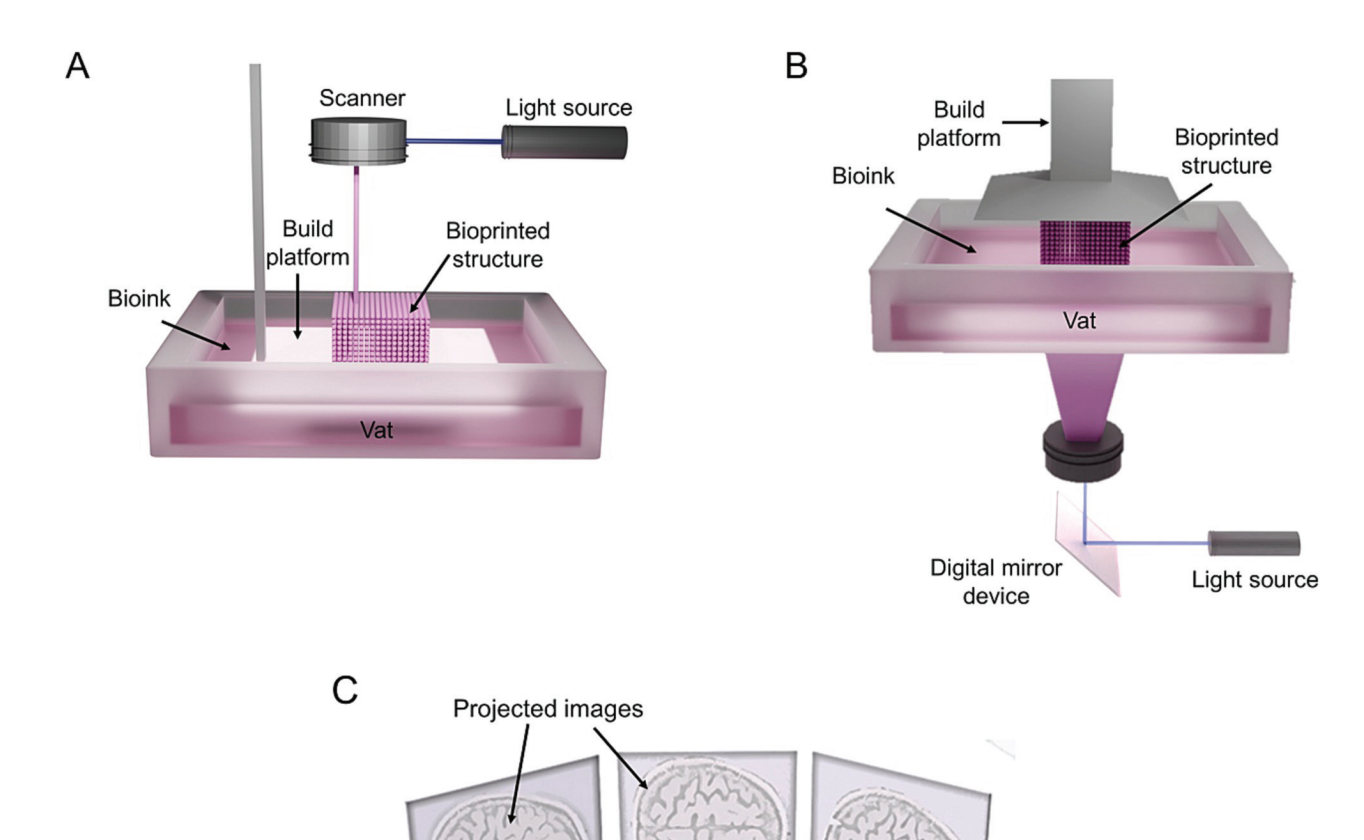


Fig. 9. Light-based vat-polymerization bioprinting methods. (A) SLA bioprinting that utilizes a UV laser beam and raster scanning to selectively cure a bioink in a point-by-point manner. (B) DLP bioprinting that uses either UV or visible light to cure the bioink in a layer-by-layer manner. (C) Volumetric bioprinting that uses the bioink reservoir connected to a rotating platform and tomographic projections of intensity-modulated light patterns at different angles for bioprinting target 3D structures.

Bioink-

Bioprinted structure

On the other hand, DLP bioprinting uses either UV or visible light prepatterned from a DLP projector to selectively cure the bioink in a layer-by-layer manner [253,325]. DLP bioprinting involves creating a structure by exposing light through a digital mask or pattern onto the surface of the bioink (Figure 9B). The digital mask may be a digital micromirror device (DMD) or a liquid-crystal display [326]. During bioprinting, for example in the top-down setup, the bioink is placed in a vat with the build platform partially submerged close to the surface of the bioink. The bioink is then exposed to light through a digital mask or pattern, causing the bioink to solidify in specific areas. The areas of the bioink that are exposed to light solidify, while the areas that are not exposed remain liquid. The build platform is then lowered, and a new layer is added on top of the previous layer. This process is repeated layer by layer until the desired structure is formed. In addition to high resolution and speed, DLP bioprinting can create small, intricate structures with high accuracy and reproducibility [314].

Both SLA and DLP bioprinting have been used for biofabrication of tissues such as liver tissue [327], cartilage tissue [328], brain [251], vascular networks [321] using photocurable hydrogels including gelatin methacryloyl (GelMA) [251,327], hyaluronic acid methacryloyl (HAMA) [251,327,329], collagen methacryloyl (ColMA) [253,330], and silk methacryloyl (SilMA) [331] as well as poly(ethylene glycol)-diacrylate (PEGDA) [321], among others.

Volumetric bioprinting, also known as tomographic 3D bioprinting, is an emerging light-assisted vat-polymerization bioprinting technique that enables the precise biofabrication of photoresponsive bioink into 3D tissue structures directly in a volumetric manner [332,333]. In volumetric bioprinting, intensity-modulated UV or visible light is projected onto a rotating vat containing the photocurable bioink using a series of filtered back projections of the desired structure. This enables simultaneous irradiation of an entire volume of the photocurable bioink from multiple angles causing the thorough penetration of illumination light throughout the entire volume of the bioink (Figure 9C). This unique feature allows for rapid and efficient biofabrication of the entire tissue construct at once, leading to a substantial reduction in overall biofabrication time [333]. Thus, volumetric bioprinting facilitates the biofabrication of geometrically complex, centimeter-scale tissue constructs with significantly increased bioprinting speed [332]. For examples, volumetric bioprinting has been used to create bone [250,334], cartilage [332], liver [335], muscle [250], auricle, and meniscus [332] tissue constructs using single cell- or organoid-embedded photoresponsive hydrogels including gelatin-based hydrogels such as GelMA [332,335] and gelatin-norbornene [333], as well as silk-based hydrogels such as silk sericin and silk fibroin [250].

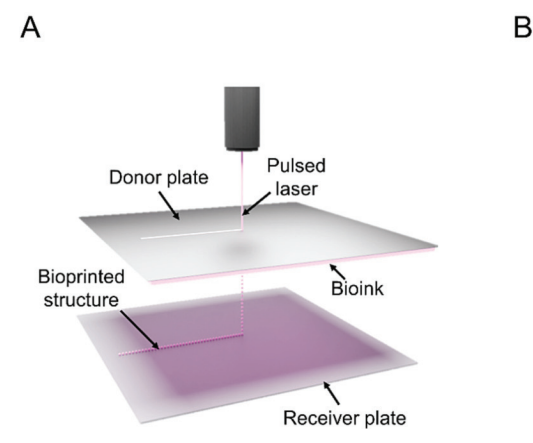
3.4. Laser-assisted bioprinting

Laser-assisted bioprinting utilizes laser pulses for precise deposition of the bioink onto a substrate. The most common laser-assisted bioprinting is based on the principle of laser-induced forward transfer that involves a pulsed laser beam, a donor substrate serving as a support for the bioink, and a receiving substrate for receiving the bioink droplets [336]. The donor substrate is typically made of laser-non-absorbing material such as glass or quartz coated with a thin layer of laserabsorbing metal such as gold or titanium and a thicker layer of the bioink. When the pulsed laser beam is directed through the donor plate and into the absorbing metal, the absorption of energy results in the generation of a high vapor pressure, which in turn propels the bioink towards the receiving substrate (Figure 10A). The receiving substrate, which typically consists of a biopolymer or cell culture medium to support cell adhesion and growth, can be moved along the x- and y-axes, enabling the continuous stacking of bioink droplets to create a 3D structure [336].

Laser-assisted bioprinting is influenced by various factors, including laser pulse energy, substrate wettability, bioprinting speed, and rheological properties of the bioink. Laser-assisted bioprinting allows processing of bioinks with high cell density and high viscosity with good degree of precision and resolution while minimizing mechanical stress on the cells [337-339]. Furthermore, this method can also be used for bioprinting of single cells and cell aggregates with remarkable accuracy and cell viability throughout the process [337,340]. Laser-assisted bioprinting has been used for the precise deposition of diverse cell types, including but not limited to fibroblasts [341], endothelial cells [342,343], mesenchymal stem cells (MSCs) [344], neural stem cells [345], and cancer cell lines such as MCF-7 cells [346]. This bioprinting method has led to some scientific progress in biofabrication of tissues including skin tissue [341,347], bone tissue [255,348], cardiac tissue [344], and corneal tissue [349], among others, using a range of hydrogels such as laminin [345], sodium alginate [343], as well as collagennanohydroxyapatite matrix [255].

3.5. Kenzan bioprinting

The Kenzan bioprinting method is an approach that utilizes cell spheroids as the fundamental building blocks [259]. It employs a specialized 3D bioprinter to precisely position these spheroids within a microneedle array. The microneedle array, referred to as 'Kenzan', typically consists of stainless-steel needles that are 160- μ m thick and spaced 500 μ m apart from one another [350]. With the help of the customized nozzle, the preformed spheroids are carefully arranged one on top of the other within each needle according to the predetermined structure. The proximity of the spheroids promotes the secretion of ECM



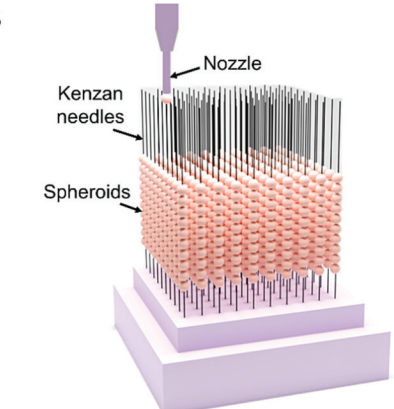


Fig. 10. Other bioprinting methods. (A) Laser-based bioprinting that uses a pulsed laser beam to generate bioink droplets, which are subsequently placed onto a receiving substrate. (B) Kenzan bioprinting that utilizes the skewing of spheroids within a microneedle array.

and facilitates cell growth (Figure 10B). Once integration and/or maturation are achieved, the tissue construct is extracted from the microneedle array for subsequent studies [259]. Of note, the deformation forces resulting from skewering the spheroids during assembly do not adversely affect cell viability, ECM production, or fusion. Kenzan bioprinting has been used to biofabricate various tissue structures such by strategically using the appropriate types of spheroids and positioning them accordingly. For examples, using the microneedle-based Kenzan method, liver-like tissues [351] and microvascular fragments [352] were successfully biofabricated by fusing spheroids formed from tissue-specific cells. Nevertheless, the Kenzan method possess certain challenges such as the precise control of spheroid size to ensure proper handling and placement during the bioprinting process and continuous monitoring of hypoxia levels within the spheroids to minimize any

negative impact on tissue growth.

4. 3D bioprinting of organoids

The bioprinting of organoids is a relatively new field and in general, two distinct approaches have been reported thus far. The first approach involves the bioprinting of undifferentiated PSCs, while the second approach focuses on bioprinting of already differentiated stem cells or the organoids themselves [353]. Although, both of these two strategies represent different avenues of research in the pursuit of advancing organoid bioprinting technology, the convergence of bioprinting and self-assembled biological building units, such as organoids, has garnered significant attention in the field of biofabrication. This approach offers the potential to develop tissue models that closely resemble organs in

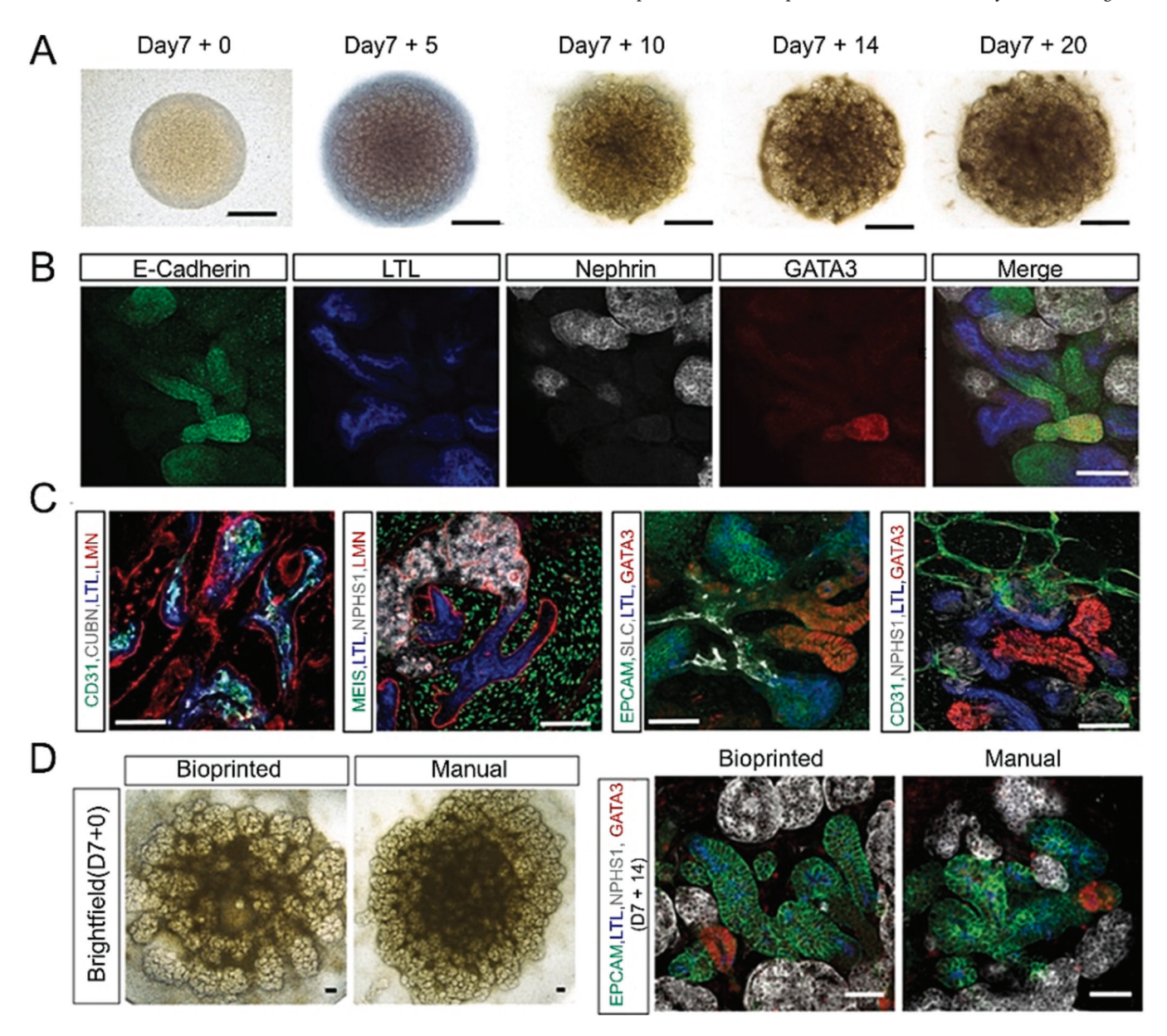


Fig. 11. Extrusion-based bioprinting of kidney organoids. (A) Bright-field images showing the spontaneous formation of nephron over the culture period. Scale bars, 800 μm. (B) Whole-mount immunofluorescence images of nephrons showing distal tubule: E-cadherin (green), proximal tubule: lotus tetragonolobus lectin (LTL, blue); podocytes: nephrin (white); connecting segment/collecting duct: GATA3 (red). Scale bar, 100 μm. (C) Whole-mount immunofluorescence staining bioprinted organoids showing podocytes (NPHS1), epithelium (EPCAM), proximal tubular segments (CD13, CUBN, LTL), tubular basement membranes (laminin; LMN), surrounding stroma (MEIS1/2/3; MEIS), thick ascending limb of distal tubule/loop of Henle (SLC12A1; SLC), distal connecting segment (GATA3), and endothelium (CD31). Scale bars, 100 μm. (D) Bright-field and whole-mount immunofluorescence images of bioprinted and manually generated kidney organoids from the same batch of hiPSC-derived intermediate mesoderm showing epithelium (EPCAM, green), proximal tubule (LTL, blue), glomeruli (NPHS1, white), connecting segment/collecting duct (GATA3, red). Scale bars, 100 μm (bright-field) and 50 μm (immunofluorescence). Reproduced with permission from Springer Nature [354].

terms of scale and functionality while combining the precise 3D spatial control provided by bioprinting with the biological resemblance achieved by utilizing organoids as building blocks and bioink components. This integration holds immense promise in establishing a humanized testing platform for personalized medicine and drug screening, enabling the development of novel models that bridge the gap between laboratory research and clinical applications. To this end, essentially all bioprinting approaches including extrusion-based, light-assisted, laser-assisted, and Kenzan bioprinting have been reported for bioprinting of PSCs or organoids.

Extrusion-based bioprinting has been adopted as a rapid and high-throughput method to generate kidney organoids with favorable reproducibility [354]. Using a cell-only bioink derived from dissociated human iPSCs (hiPSCs) at the mesoderm developmental stage, precise and rapid extrusion onto Transwell plates was achieved. The automated bioprinting process enabled precise control over biophysical properties such as cell number and organoid size, resulting in uniform self-organizing kidney organoids. BFM and whole-mount LSCM were used to demonstrate that extrusion-based bioprinting facilitated the automated biofabrication of self-organizing kidney organoids which were comparable to those generated by conventional method at the level of morphology, cell composition, and gene expressions (Figure 11). To

further explore the impact of organoid conformation on morphology, the authors created 'lined' organoids instead of 'dot' organoids using the same number of starting cells. Organoids with increasing length but the same number of starting cells displayed thinner tissues and increased nephron numbers. Furthermore, the bioprinted kidney organoids were assessed for nephrotoxicity by testing various drugs including doxorubicin, amikacin, tobramycin, gentamicin, neomycin, and streptomycin. It is important to note that this study only utilized a single nephron progenitor cell population at the intermediate mesoderm stage, resulting in the kidney organoids primarily consisting of derivatives of the metanephric mesenchyme, lacking cell populations from the ureteric bud, as well as a functional vasculature.

In an another study, extrusion-based bioprinting, named bioprinting-assisted tissue emergence (BATE), was employed for guiding tissue morphogenesis at physiologically relevant scales directly within highly permissive ECMs such as Matrigel, collagen I, and methylcellulose [355]. In BATE, stem cells and organoids were utilized as building blocks that form interconnected and dynamic cellular constructs within the ECM (Figure 12). They were directed to conform to predefined geometries and constraints, thereby enabling the controlled development of tissue structures. The versatility of BATE in guiding the macroscale self-organization of primary cells derived from human tissues was

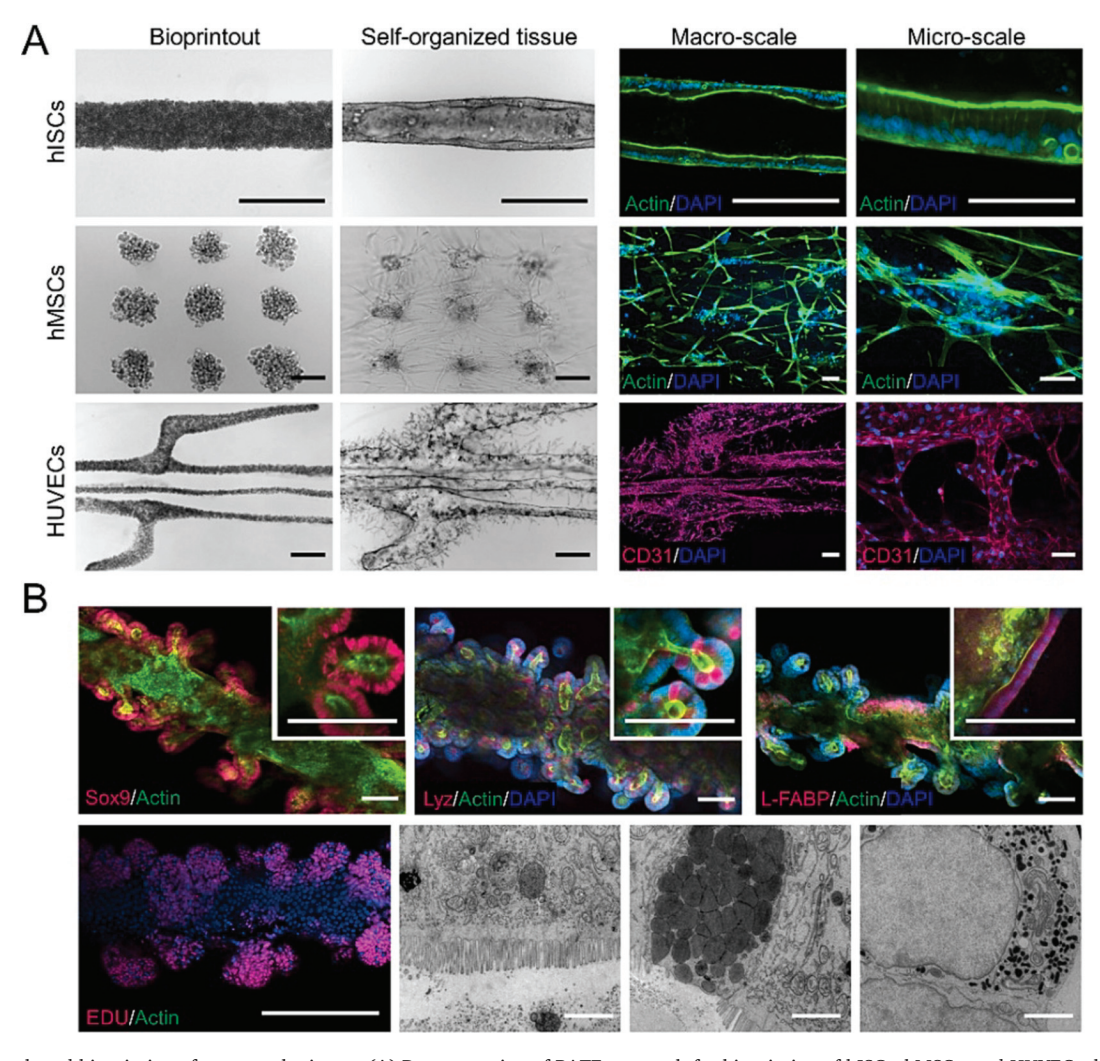


Fig. 12. Extrusion-based bioprinting of macroscale tissues. (A) Demonstration of BATE approach for bioprinting of hISCs, hMSCs, and HUVECs that self-organized into respective organoids and then into large-scale tissues, followed by fluorescence confocal images of macroscopic and microscopic tissue structures. Scale bars, 500 μm (bright-field), 250 μm (macroscale fluorescence), and 75 μm (microscale fluorescence). (B) Fluorescence confocal images of intestinal tubes, showing the expression of F-actin, Sox9, Lyz, or L-FABP and Edu by intestinal stem and progenitor cells, Paneth cells and enterocytes. Scale bar, 200 μm. Followed by TEM of an intestinal tube sections showing enterocytic brush border, goblet cells, and enteroendocrine cells. Scale bars, 2 μm. Reproduced with permission from Springer Nature [355].

demonstrated by bioprinting three distinct cell types, namely human intestinal stem cells (hISCs), human MSCs (hMSCs), and human umbilical vein endothelial cells (HUVECs). hISCs were bioprinted in a linear pattern within a Matrigel/collagen-precursor. The BFM and LSCM imaging showed that the hISCs underwent morphological transformations and formed interconnected and polarized epithelial tubes within the crosslinked matrix over the period of several days. When hMSCs were precisely positioned within a Matrigel/collagen matrix, they exhibited remarkable migration and invasion capabilities into the surrounding ECM, ultimately forming a fibrous connective tissue-like structure. Similarly, bioprinted HUVECs self-organized into branched vascular tubes that possessed a perfusable lumen. Furthermore, when these HUVECs were bioprinted in collagen I and stimulated with a high concentration of vascular endothelial growth factor (VEGF), they displayed the ability to form de novo capillaries (Figure 12A). Next, mouse intestinal stem cells (mISCs) were bioprinted in Matrigel and supplemented with a defined cocktail of growth factors (epidermal growth factor, Noggin, and R-spondin (ENR)), forming organoids that possess crypts and villus-like compartments resembling the epithelium of the small intestine in vivo. Guided by the imposed cylindrical geometry, the bioprinted mISCs initially condensed into a thick tubular structure without a lumen. However, they expanded as colonies and fused together after some time, resulting in the formation of a polarized and lumenized epithelial tissue (Figure 12B). The cellular composition of the bioprinted intestinal tissues were analyzed by immunostaining of 8-day-old tubes and revealed the presence of putative crypts (marked by SRY-related HMG box (SOX) family of transcription factor 9, Sox9) containing Paneth cells (lysozyme, Lyz), as well as a villus-like domain that expressed the enterocyte marker (liver-fatty acid binding protein, L-FABP)). Proliferative cells, identified by their labeling with the thymidine analogue 5-ethynyl-2'-deoxyuridine (EdU), were exclusively localized in the crypts. Furthermore, TEM provided evidence of the presence of mature differentiated cell types within the tubes, including enterocytes with a distinct apical brush border, mucus-producing goblet cells, and enteroendocrine cells. Thus, these findings highlight the potential of BATE to precisely guide the organization and development of various cell types for creating complex and functional tissue structures that closely resemble native physiological conditions.

In a recent study, volumetric bioprinting has been used to biofabricate liver tissue constructs using human liver epithelial organoids obtained from adult stem cells found in intrahepatic bile ducts [335]. These hepatic organoids were epithelial in nature, forming a cyst-like structure with an inner hollow lumen surrounded by a thin cell layer. Hepatic organoids were embedded in GelMA consisting of LAP and placed in a cylindrical borosilicate glass vial. The bioprinting process was induced by a laser beam at 405 nm directed onto a DMD that was modulated into tomographic projections which were then projected into the glass vials, facilitating the creation of liver tissue constructs. GelMA bioink was further supplemented with iodixanol to optically tune the bioink for enhanced bioprinting resolution in the presence of cellular structures. The bioprinted hepatic organoids underwent hepatocytic differentiation and demonstrated essential functions characteristic of the human liver. Notably, these bioprinted liver tissues exhibited albumin synthesis, liver-specific enzyme activity, and remarkably acquired a native-like polarization. The expression of organoid polarization markers, including hepatocyte nuclear factor 4α (HNF4 α), multidrug resistance protein 1 (MDR-1), albumin, and cytochrome P450 3A4 activity, was observed in the bioprinted liver tissue using LSCM. Moreover, the bioprinted liver tissue released comparable levels of various liver transaminases, such as aspartate transaminase (ASAT) involved in amino acid metabolism, gamma-glutamyl transferase (GGT) involved in drug and xenobiotic detoxification, and glutamate dehydrogenase (GLDH) involved in the urea cycle. These findings indicated that the volumetrically bioprinted liver tissue exhibited functional characteristics similar to those of native liver tissue, showcasing its potential as a valuable tool in drug metabolism studies and liver disease modeling.

Kenzan bioprinting was utilized to fuse numerous liver bud (LB)-like spheroids, resulting in the rapid creation of scaffold-free and scalable liver-like tissue [351]. LB-like spheroids were generated using early lineage hepatocytes, HUVECs, and MSCs. These LB-like spheroids were subsequently skewed in a needle-array system to secure the LB-like spheroids in a 3D arrangement, allowing for the biofabrication of liver-like tissue with intricate geometries. This approach facilitated immediate culture circulation after bioprinting, preventing the development of an ischemic environment *in vitro*. Fluorescence microscopy showed that the resulting liver-like tissue demonstrated self-organization *in vitro*, and when transplanted onto a rat liver, it successfully survived within a 100-µm range.

A recent study has introduced an orthogonally induced differentiation (OID) approach that allowed rapid programming and patterning of hiPSCs, leading to the generation of genetically programmed human stem cells, organoids, and 3D-bioprinted organ-specific tissues with precise composition and organization within a short timeframe [356]. In the OID approach, doxycycline-induced overexpression of transcription factors was shown to operate autonomously in pre-programmed hiPSCs to generate specific cell types, independent of differentiation induced by culture media. Inducible endothelial cells (iEndos) were generated by the overexpression of the ETS Variant Transcription Factor 2 (ETV2), known for driving rapid and efficient directed differentiation of hiPSCs into vascular endothelial cells. Inducible neurons (iNeurons) were generated by upregulating Neurogenin 1 or co-expression of neurogenins, facilitating the rapid generation of neurons from hiPSCs. The OID approach was applied to randomly pooled or multicore-shell embryoid bodies, resulting in the construction of multicellular and spatially patterned vascularized and multicore-shell cortical organoids within days. Vascularized cortical organoids were cleared and immunolabelled using an immunolabelling-enabled DISCO method, and imaged using a confocal microscope. Moreover, the OID approach was coupled with multimaterial 3D bioprinting using matrix-free, dense cellonly bioinks, wild type (WT) hiPSCs, inducible-TF hiPSCs-, iEndos, and iNeurons. Bioprinted WT hiPSC filaments formed a neuroectoderm filament when differentiated in neural induction medium containing doxycycline. Bioprinted iEndo filaments exhibited vasculogenesis, forming a microvascular network over time, while bioprinted iNeuron filaments differentiated into densely packed neuronal nuclear protein (NeuN)⁺ neurons, creating a network of protruding neuron-specific class III beta-tubulin (Tuj1)⁺ neurites. Thus, the study showcased the potential of OID to generate vascularized cortical organoids in pooled and multicore-shell configurations, as well as the creation of 3D cortical tissues composed of multiple cell types patterned in spatially distinct regions.

Thus, 3D imaging of bioprinted organoids is crucial because it allows for comprehensive visualization and analyses of their complex spatial structures and internal dynamics. By capturing the 3D geometries, cellular organizations, and tissue morphologies, the imaging techniques provide essential details about the development, maturation, and functionality of bioprinted organoids. These also allow the assessment of cell-cell interactions and tissue architecture within the bioprinted constructs, facilitating a better understanding of their biological characteristics and potential applications in regenerative medicine, drug discovery, and disease modeling.

5. 3D imaging in advancing organoid bioprinting

3D imaging plays a crucial role in advancing bioprinting technology and ensuring the successful bioprinting of tissue scaffolds with high fidelity and accuracy. The success of bioprinting depends on the precision and reliability of the process, and 3D imaging aids in evaluating the fidelity and accuracy of the bioprinting process and ensures the quality and reproducibility of bioprinted tissue scaffolds. 3D imaging technologies, such as OCT, have been integrated with 3D bioprinting platforms to enable the visualization of the bioprinting process in real-time. This,

in fact, allows the continuous monitoring of the precise deposition of bioink, ensuring that the bioprinted layers align correctly and that there are no defects or misalignments. Adjustments to bioprinting parameters can be made promptly if any irregularities are observed during the imaging process. For example, in a recent study, pneumatic-based extrusion bioprinter equipped with a swept-source OCT (P-OCT) was developed for real-time processing monitoring and quality evaluation during the bioprinting of the scaffolds using polycaprolactone and hydrogel composed of gelatin and alginate [357]. In the P-OCT system, an OCT probe, consisted of a wavelength swept laser source with a central wavelength of 1310 nm, a bandwidth of 105 nm, and a 50-kHz A-scan rate, was positioned alongside the printing nozzle (500-µm inner diameter), enabling OCT imaging to be carried out in an alternating fashion with the layer-by-layer bioprinting process. This system was specially designed for imaging large-volume constructs of 20 mm (x) \times 20 mm (y) \times 9.3 mm (z) using a wide-field and full-depth imaging strategies, yielding a measured axial resolution of 7.2 µm and a lateral resolution of 15.0 µm. For wide-field imaging, the checkerboard scanning protocol was employed to achieve lateral image mosaic from which overlapping areas were extracted, facilitating precise lateral registration using point cloud alignment. On the other hand, full-depth imaging was achieved by applying the stacking scanning protocol along with the gray value maximum method for longitudinal image mosaic. Moreover, an image-processing script was created using wide-field and full-depth OCT data that allowed in situ assessment of filament size, layer thickness, and pore size. The 3D wide-field and full-depth imaging of the scaffold was achieved, composed of 270 sub-datasets and calculated size of 20.500 mm (x) \times 20.380 mm (y) \times 9.351 mm (z) which was close to the dimensions depicted by micro-computed tomography (20.536 mm (x) \times 20.400 mm (y) \times 9.385 mm (z)). Thus, P-OCT facilitated real-time process monitoring and comprehensive quantitative and qualitative evaluations by offering various volumetric parameters, including material volume, volume porosity, and pore connectivity throughout the 3D bioprinting process, ensuring high structural fidelity.

In an another study, a multi-material bioprinting platform with integrated OCT was developed for real-time volumetric imaging, error-identification, and 3D reconstruction [358].

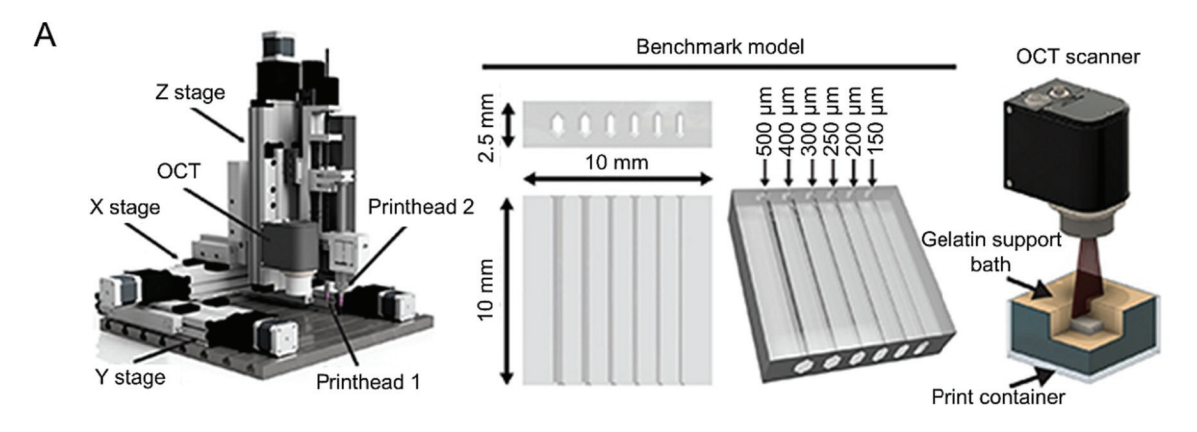
It consisted of dual-extruder 3D bioprinter equipped with an integrated OCT system, enabling real-time imaging during Freeform Reversible Embedding of Suspended Hydrogels (FRESH) bioprinting (a type of embedded bioprinting) using collagen I bioink and clear gelatin microparticle support bath. The 3D bioprinter employed precision translation stages to facilitate the convenient mounting of the OCT scan head while ensuring repeatable positioning with an accuracy of $\sim 8 \mu m$ for sequential imaging and also achieving high bioprinting speeds of up to 40 mm s⁻¹. A clear gelatin microparticle support bath was prepared using iodixanol, and titanium dioxide was incorporated into the collagen bioink as a contrast agent that significantly enhanced the signal-to-noise ratio of the bioink. A benchmark model, featuring internal channels of different widths ranging from 150–500 μ m, individual filaments of ~ 87 µm in diameter and an overall construct size of up to 10 mm, was created to evaluate bioprinter performance, resolution capabilities, and OCT imaging quality. Furthermore, a custom MATLAB code was created that interleaves the G-code for the gelatin microparticle support bath with the G-code for the structure to be bioprinted, enabling the bioprinting of the structure within the gelatin microparticle support bath. The process was initiated with the deposition of the gelatin microparticle support bath, followed by the bioprinting of a section of the structure using highcontrast collagen. The OCT scan head was then positioned over the bioprinted structure to capture an image. OCT image stacks of the bioprinted structure were acquired at regular z-height intervals throughout the entire bioprinting process. Subsequently, all the acquired OCT stacks were then registered in 3D and merged to generate a comprehensive composite OCT image stack. When the OCT image captured at the end of the bioprinting process was compared with the composite OCT image acquired through in-process OCT imaging, a significant improvement was observed in image signal quality, especially as the thickness increases (Figure 13). Enhanced OCT imaging quality throughout the bioprinting process and the increased signal-to-noise ratio achieved through the use of high-contrast collagen bioink allowed for a quantitative evaluation of both the external and internal characteristics of the bioprinted structures such as the width of the inner and outer walls and the spacing between filaments. The OCT images obtained after release showed that the bioprinting of the gelatin microparticle support bath did not alter the dimensions of the final bioprinted structures, thus illustrating the remarkable geometric precision and accuracy of the bioprinting process while highlighting the capability the FRESH bioprinting and sequential OCT imaging for real-time 3D imaging and dimensional analysis. Moreover, the use of a high-contrast collagen bioink along with a clear gelatin microparticle support bath allowed for the identification assessment of print defects and internal errors.

Likewise, a recent study has demonstrated the utilization of photoacoustic microscopy (PAM, a high-resolution implementation of PAT) for label-free visualization of 3D-bioprinted vascular channels created via DLP-based bioprinting by us [219]. The custom-built DLP-based 3D printer, equipped with DMD chip (resolution: 1280×800 pixels) and a projector projecting patterns with visible light of 25 mW cm⁻², was employed to fabricate vascular channels. Various vascular channel designs, including Y-shaped channels, single-loop channels, and complex dodecahedron-patterned microchannels were fabricated at a speed of 10 to 70 μm s⁻¹ and with a layer height of 350 μm using PEGDA, GelMA, or a bioink consisting of GelMA and HAMA along with Ru/SPS as the photoinitiator. The study subsequently examined the imaging capabilities of optical resolution-PAM (OR-PAM) and acoustic resolution-PAM (AR-PAM) in visualizing 3D-bioprinted vascular channels and shown that AR-PAM achieved greater penetration depth and enabled superior visualization of vascular channels within volumetric structures compared to OR-PAM. Indeed, OR-PAM offered a penetration depth of \sim 1 mm and a lateral resolution of \sim 3.7 μ m, whereas AR-PAM could achieve a penetration depth beyond the ballistic regime and a lateral resolution of ~ 50 μm . Furthermore, PAM was employed to quantitatively assess the blood oxygenation within the 3D-bioprinted vascular channels. The results revealed that thrombi exhibited lower oxygenation levels compared to normal blood, highlighting the capability of AR-PAM to detect changes in oxygen saturation of hemoglobin within bioprinted vascular channels perfused with blood with different oxygenation levels (0.93-0.55). The results revealed that thrombi exhibited lower oxygenation levels compared to normal blood, indicating the capability of PAM to quantify the blood oxygenation of thrombotic regions. In fact, PAM holds a great potential for their applications in 3D bioprinting and functionality measurements, particularly in vitro studies on a wide range of vascular diseases.

6. Conclusions and future perspectives

Imaging techniques hold significant promise in the characterizations and studies of organoid biology, both conventionally generated organoids and 3D-bioprinted organoids. These techniques enable the visualization of organoid structures, cellular dynamics, molecular interactions, and functional properties. By providing detailed insights into the spatial organization and behavior of organoids, imaging facilitates a deeper understanding of their biology and potential applications.

Currently, a range of imaging modalities is employed for imaging organoids, including primarily TEM, SEM, BFM, fluorescence microscopy, LSCM, MPM, FLIM, LSM, SRFM, OCT, and PAT. Each technique offers unique capabilities and advantages, allowing researchers to examine different aspects of organoid structures and functions. While current imaging techniques play an important role in facilitating our comprehension of organoid structures, there is a need for further improvement in spatial resolution for 3D-bioprinted organoids. Higher-resolution imaging would allow for the visualization of finer cellular details and subcellular structures within the organoids. Furthermore,



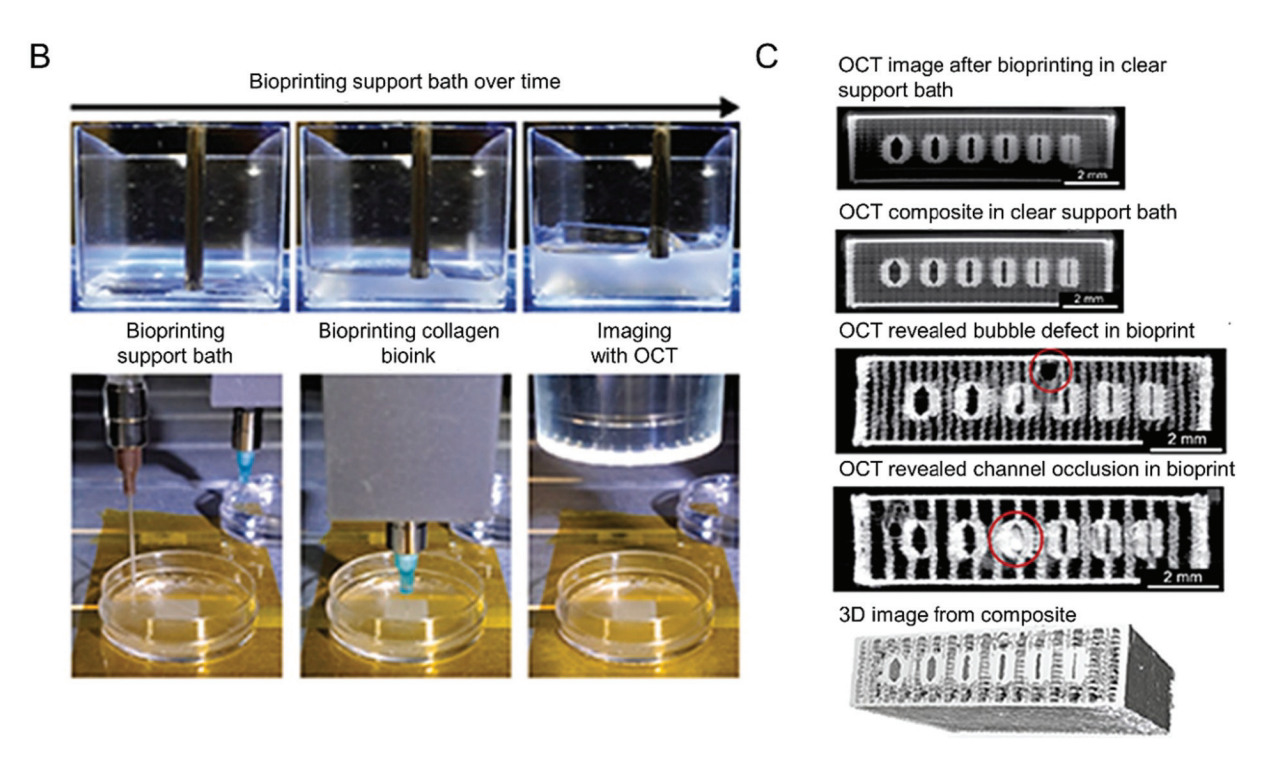


Fig. 13. Integration of OCT into the FRESH bioprinting platform. (A) 3D bioprinter with dual extruders and an OCT scan head, a benchmark model with internal channels of varying widths and schematics showing the OCT imaging of a FRESH-bioprinted structure within the gelatin microparticle support bath. (B) Time-lapse images of bioprinting of gelatin microparticle support bath followed by sequential process of bioprinting of the support bath, a collagen structure within the support bath, and OCT imaging. (C) OCT imaging of bioprinted structure within clear gelatin microparticle support bath after completion of bioprinting process and inprocess OCT imaging and the composite OCT image obtained through in-process OCT imaging, followed by bioprinting errors such as air bubble and channel occlusion detected by in-process OCT imaging and 3D reconstruction of composite OCT images of a benchmark model. Scale bars, 2 mm. Reproduced with permission from IOP Publishing [358].

integrating multiple imaging modalities can provide a more comprehensive understanding of bioprinting process and organoid biology. For example, a 3D bioprinting platform with the integrated 3D imaging capacity serves as an essential tool in bioprinting process, playing a vital role in assessing, ensuring quality control, and optimizing the bioprinting process through real-time visualization, cell distribution and viability assessment and tissue morphology characterization while assuring the reproducibility. Additionally, it facilitates the evaluations of the functionalities of the bioprinted tissue structures. Combining imaging techniques such as fluorescence imaging, LSCM/MPM, FLIM, and functional photoacoustic imaging with bioprinters could offer complementary information relating to organoid structure, molecular composition, and cellular dynamics. Monitoring organoid development and behavior over time is essential for studying their dynamic nature.

As 3D-bioprinted organoids hold the potential to create tissue models that closely emulate organs in terms of scale and functionality, and thus

are intended for further subsequent experimentation or transplantation. Therefore, developing imaging techniques that enable long-term and non-invasive imaging along with live imaging capabilities, would greatly enhance the understanding of their growth, differentiation, and response to stimuli. Furthermore, integration of imaging with functional assays, such as gene expression assessments, cellular activity measurements, or drug response studies, would enable more comprehensive characterizations of 3D-bioprinted organoids and providing insights into the functional properties and physiological relevance of the organoids.

In summary, imaging techniques are essential tools for the characterization of 3D-bioprinted organoids. Advancements in imaging resolution, multi-modal imaging approaches, long-term, and non-destructive imaging, as well as integration with functional assays will further improve the understanding of organoid biology and accelerate their applications in regenerative medicine, disease modeling, and drug discovery. Continued research and development in imaging

technologies will undoubtedly contribute to the progress of 3D-bioprinted organoids in the future.

Declaration of Competing Interest

The authors declare that they have no known competing financial interests or personal relationships that could have appeared to influence the work reported in this paper.

Acknowledgements

The work is supported by the National Institutes of Health (R21EB025270, R21EB030257, UH3TR003274, R01HL153857, R01HL165176, R01HL166522, R01CA282451, R56EB034702), the National Science Foundation (CBET-EBMS-1936105, CISE-IIS-2225698), Chan-Zuckerberg Initiative (2022-316709), and the Brigham Research Institute, all to Y.S.Z; National Institutes of Health (NIH) (R21EB027981, R21EB027304, RF1NS115581 (BRAIN Initiative), R01NS111039, R01EB028143, R21EB027981, and R01EB031629), National Science Foundation CAREER award 2144788, and Chan Zuckerberg Initiative Grant 2020-226178, all to J.Y. The work was also assisted by the Spanish Ministry of Economy, Industry, and Competitiveness (PID2022-139746OB-I00/AEI/10.13039/501100011033).

References

- [1] M. Hofer, M.P. Lutolf, Engineering organoids, Nat. Rev. Mater. 6 (5) (2021) 402–420.
- [2] K.E. Boonekamp, T.L. Dayton, H. Clevers, Intestinal organoids as tools for enriching and studying specific and rare cell types: advances and future directions, J Mol Cell Biol 12 (8) (2020) 562–568.
- [3] X. Yin, et al., Niche-independent high-purity cultures of Lgr5+ intestinal stem cells and their progeny, Nat Methods 11 (1) (2014) 106–112.
- [4] A.E. Shyer, et al., Bending gradients: how the intestinal stem cell gets its home, Cell 161 (3) (2015) 569–580.
- [5] H. Clevers, Modeling Development and Disease with Organoids, Cell 165 (7) (2016) 1586–1597.
- [6] Z. Zhao, et al., Organoids. Nature Reviews Methods Primers 2 (1) (2022) 94.
- [7] A. Akhtar, The flaws and human harms of animal experimentation, Camb Q Healthc Ethics 24 (4) (2015) 407–419.
- [8] T.G. Krieger, et al., Single-cell analysis of patient-derived PDAC organoids reveals cell state heterogeneity and a conserved developmental hierarchy, Nat. Commun. 12 (1) (2021) 5826.
- [9] A. Fatehullah, S.H. Tan, N. Barker, Organoids as an in vitro model of human development and disease, Nat. Cell Biol. 18 (3) (2016) 246–254.
- [10] S. Yui, et al., Functional engraftment of colon epithelium expanded in vitro from a single adult Lgr5 stem cell, Nat Med 18 (4) (2012) 618–623.
- [11] N. Georgakopoulos, et al., Long-term expansion, genomic stability and in vivo safety of adult human pancreas organoids, BMC Dev Biol 20 (1) (2020) 4.
- [12] Miranda, C.C. and J.M.S. Cabral, Organoids for cell therapy and drug discovery, in Precision Medicine for Investigators, Practitioners and Providers, J. Faintuch and S. Faintuch, Editors. 2020, Academic Press. p. 461-471.
- [13] M.A. Lancaster, M. Huch, Disease modelling in human organoids, Dis Model Mech 12 (7) (2019).
- [14] J. Kim, B.-K. Koo, J.A. Knoblich, Human organoids: model systems for human biology and medicine, Nat. Rev. Mol. Cell Biol. 21 (10) (2020) 571–584.
- [15] M.H. Geurts, H. Clevers, CRISPR engineering in organoids for gene repair and disease modelling, Nature Reviews Bioengineering 1 (1) (2023) 32–45.
- [16] A. Al Shihabi, et al., Personalized chordoma organoids for drug discovery studies. 8 (7) (2022).
- [17] W. Hu, M.A. Lazar, Modelling metabolic diseases and drug response using stem cells and organoids. Nat. Rev. Endocrinol. 18 (12) (2022) 744–759.
- [18] S. Bose, H. Clevers, X. Shen, Promises and Challenges of Organoid-Guided Precision Medicine, Med 2 (9) (2021) 1011–1026.
- [19] Z. Zhou, L. Cong, X. Cong, Patient-Derived Organoids in Precision Medicine: Drug Screening, Organoid-on-a-Chip and Living Organoid Biobank, Front Oncol 11 (2021) 762184.
- [20] A. Ootani, et al., Sustained in vitro intestinal epithelial culture within a Wntdependent stem cell niche, Nat Med 15 (6) (2009) 701–706.
- [21] T. Sato, et al., Single Lgr5 stem cells build crypt-villus structures in vitro without a mesenchymal niche, Nature 459 (7244) (2009) 262–265.
- [22] T. Sato, et al., Long-term Expansion of Epithelial Organoids From Human Colon, Adenoma, Adenocarcinoma, and Barrett's Epithelium, Gastroenterology 141 (5) (2011) 1762–1772.
- [23] J.R. Spence, et al., Directed differentiation of human pluripotent stem cells into intestinal tissue in vitro, Nature 470 (7332) (2011) 105–109.
- [24] M.J. Workman, et al., Engineered human pluripotent-stem-cell-derived intestinal tissues with a functional enteric nervous system, Nat. Med. 23 (1) (2017) 49–59.

- [25] A. Mithal, et al., Generation of mesenchyme free intestinal organoids from human induced pluripotent stem cells, Nat. Commun. 11 (1) (2020) 215.
- [26] Q. Wang, et al., Applications of human organoids in the personalized treatment for digestive diseases, Signal Transduct. Target. Ther. 7 (1) (2022) 336.
- [27] M. Funata, et al., The promise of human organoids in the digestive system, Cell Death Differ. 28 (1) (2021) 84–94.
- [28] F. Perrone, M. Zilbauer, Biobanking of human gut organoids for translational research, Exp. Mol. Med. 53 (10) (2021) 1451–1458.
- [29] J. Lu, et al., Characterization of an in vitro 3D intestinal organoid model by using massive RNAseq-based transcriptome profiling, Sci. Rep. 11 (1) (2021) 16668.
- [30] B.E. Mead, et al., Screening for modulators of the cellular composition of gut epithelia via organoid models of intestinal stem cell differentiation, Nat. Biomed. Eng. 6 (4) (2022) 476–494.
- [31] C. Bouffi, et al., In vivo development of immune tissue in human intestinal organoids transplanted into humanized mice, Nat. Biotechnol. (2023).
- [32] S. Kim, et al., Tissue extracellular matrix hydrogels as alternatives to Matrigel for culturing gastrointestinal organoids, Nat. Commun. 13 (1) (2022) 1692.
- [33] Engineering carcinogenesis in intestinal organoids, Nat. Rev. Gastroenterol. Hepatol. 12 (4) (2015).
- [34] J.Y. Co, et al., Controlling the polarity of human gastrointestinal organoids to investigate epithelial biology and infectious diseases, Nat. Protoc. 16 (11) (2021) 5171–5192.
- [35] H. Stower, Modeling kidney disease with organoids, Nat. Med. 25 (4) (2019).
- [36] R. Nishinakamura, Human kidney organoids: progress and remaining challenges, Nat. Rev. Nephrol. 15 (10) (2019) 613–624.
- [37] M. Shi, et al., Human ureteric bud organoids recapitulate branching morphogenesis and differentiate into functional collecting duct cell types, Nat. Biotechnol. 41 (2) (2023) 252–261.
- [38] A.A. Palakkan, et al., Production of kidney organoids arranged around single ureteric bud trees, and containing endogenous blood vessels, solely from embryonic stem cells, Sci. Rep. 12 (1) (2022) 12573.
- [39] M. Koning, et al., Vasculogenesis in kidney organoids upon transplantation. npj, Regen. Med. 7 (1) (2022) 40.
- [40] J.L. Davis, et al., Single-cell multiomics reveals the complexity of TGFβ signalling to chromatin in iPSC-derived kidney organoids, Communications Biology 5 (1) (2022) 1301.
- [41] R. Morizane, et al., Nephron organoids derived from human pluripotent stem cells model kidney development and injury, Nat. Biotechnol. 33 (11) (2015) 1193–1200.
- [42] Y. Yuan, et al., Generation of mitochondria-rich kidney organoids from expandable intermediate mesoderm progenitors reprogrammed from human urine cells under defined medium, Cell Biosci. 12 (1) (2022) 174.
- [43] B.S. Freedman, et al., Modelling kidney disease with CRISPR-mutant kidney organoids derived from human pluripotent epiblast spheroids, Nat. Commun. 6 (1) (2015) 8715.
- [44] A.-N. Cho, et al., Microfluidic device with brain extracellular matrix promotes structural and functional maturation of human brain organoids, Nat. Commun. 12 (1) (2021) 4730.
- [45] T. Sharf, et al., Functional neuronal circuitry and oscillatory dynamics in human brain organoids, Nat. Commun. 13 (1) (2022) 4403.
- [46] A. Fiorenzano, et al., Single-cell transcriptomics captures features of human midbrain development and dopamine neuron diversity in brain organoids, Nat. Commun. 12 (1) (2021) 7302.
- [47] J.S. Fleck, et al., Inferring and perturbing cell fate regulomes in human brain organoids, Nature (2022).
- [48] I. Kelava, et al., Androgens increase excitatory neurogenic potential in human brain organoids, Nature 602 (7895) (2022) 112–116.
- [49] Y. Wang, et al., Modeling human telencephalic development and autismassociated SHANK3 deficiency using organoids generated from single neural rosettes. Nat. Commun. 13 (1) (2022) 5688.
- [50] G. Quadrato, et al., Cell diversity and network dynamics in photosensitive human brain organoids, Nature 545 (7652) (2017) 48–53.
- [51] J.A. Bagley, et al., Fused cerebral organoids model interactions between brain regions, Nat. Methods 14 (7) (2017) 743–751.
- [52] L. Wang, et al., Loss of NARS1 impairs progenitor proliferation in cortical brain organoids and leads to microcephaly, Nat. Commun. 11 (1) (2020) 4038.
- [53] P. Saglam-Metiner, et al., Spatio-temporal dynamics enhance cellular diversity, neuronal function and further maturation of human cerebral organoids, Communications Biology 6 (1) (2023) 173.
- [54] A.A. Mansour, et al., An in vivo model of functional and vascularized human brain organoids, Nat. Biotechnol. 36 (5) (2018) 432–441.
- [55] B. Cakir, et al., Engineering of human brain organoids with a functional vascularlike system, Nat. Methods 16 (11) (2019) 1169–1175.
- [56] S. Bian, et al., Genetically engineered cerebral organoids model brain tumor formation, Nat. Methods 15 (8) (2018) 631–639.
- [57] M.A. Lancaster, et al., Cerebral organoids model human brain development and microcephaly, Nature 501 (7467) (2013) 373–379.
- [58] S.-E. Lee, et al., Zika virus infection accelerates Alzheimer's disease phenotypes in brain organoids, Cell Death Discovery 8 (1) (2022) 153.
 [59] R.A. Samarasinghe, et al., Identification of neural oscillations and epileptiform
- changes in human brain organoids, Nat. Neurosci. 24 (10) (2021) 1488–1500. [60] E. Karzbrun, et al., Human brain organoids on a chip reveal the physics of folding,
- Nat. Phys. 14 (5) (2018) 515–522.
- [61] S. Velasco, et al., Individual brain organoids reproducibly form cell diversity of the human cerebral cortex, Nature 570 (7762) (2019) 523–527.

- [62] J. Brás, et al., Establishment and characterization of human pluripotent stem cells-derived brain organoids to model cerebellar diseases, Sci. Rep. 12 (1) (2022) 12513
- [63] J. Xu, et al., Generation of neural organoids for spinal-cord regeneration via the direct reprogramming of human astrocytes, Nat. Biomed. Eng. 7 (3) (2023) 253–269.
- [64] M.-F. Ho, et al., Single cell transcriptomics reveals distinct transcriptional responses to oxycodone and buprenorphine by iPSC-derived brain organoids from patients with opioid use disorder, Mol. Psychiatry (2022).
- [65] E. Di Lullo, A.R. Kriegstein, The use of brain organoids to investigate neural development and disease, Nat. Rev. Neurosci. 18 (10) (2017) 573–584.
- [66] D. Hendriks, et al., Engineered human hepatocyte organoids enable CRISPRbased target discovery and drug screening for steatosis, Nat. Biotechnol. (2023).
- [67] L. Sun, et al., Modelling liver cancer initiation with organoids derived from directly reprogrammed human hepatocytes, Nat. Cell Biol. 21 (8) (2019) 1015–1026.
- [68] N. Tanimizu, et al., Generation of functional liver organoids on combining hepatocytes and cholangiocytes with hepatobiliary connections ex vivo, Nat. Commun. 12 (1) (2021) 3390.
- [69] H.S. Lee, et al., Integrative analysis of multiple genomic data from intrahepatic cholangiocarcinoma organoids enables tumor subtyping, Nat. Commun. 14 (1) (2023) 237.
- [70] D. Hendriks, et al., Establishment of human fetal hepatocyte organoids and CRISPR-Cas9-based gene knockin and knockout in organoid cultures from human liver, Nat. Protoc. 16 (1) (2021) 182–217.
- [71] Y. Guan, et al., A human multi-lineage hepatic organoid model for liver fibrosis, Nat. Commun. 12 (1) (2021) 6138.
- [72] J. Lee, et al., Advances in liver organoids: model systems for liver disease, Arch. Pharm. Res. 45 (6) (2022) 390–400.
- [73] L. Broutier, et al., Culture and establishment of self-renewing human and mouse adult liver and pancreas 3D organoids and their genetic manipulation, Nat. Protoc. 11 (9) (2016) 1724–1743.
- [74] G. Sorrentino, et al., Mechano-modulatory synthetic niches for liver organoid derivation, Nat. Commun. 11 (1) (2020) 3416.
- [75] G. Belenguer, et al., RNF43/ZNRF3 loss predisposes to hepatocellular-carcinoma by impairing liver regeneration and altering the liver lipid metabolic groundstate, Nat. Commun. 13 (1) (2022) 334.
- [76] Y. Chen, et al., Acute liver steatosis translationally controls the epigenetic regulator MIER1 to promote liver regeneration in a study with male mice, Nat. Commun. 14 (1) (2023) 1521.
- [77] M.A. Branco, et al., Human multilineage pro-epicardium/foregut organoids support the development of an epicardium/myocardium organoid, Nat. Commun. 13 (1) (2022) 6981.
- [78] L. Drakhlis, et al., Human heart-forming organoids recapitulate early heart and foregut development. Nat. Biotechnol. 39 (6) (2021) 737–746.
- [79] J. Lee, et al., In vitro generation of functional murine heart organoids via FGF4 and extracellular matrix, Nat. Commun. 11 (1) (2020) 4283.
- [80] D.J. Richards, et al., Human cardiac organoids for the modelling of myocardial infarction and drug cardiotoxicity, Nat. Biomed. Eng. 4 (4) (2020) 446–462.
- [81] Q. Lyu, et al., A soft and ultrasensitive force sensing diaphragm for probing cardiac organoids instantaneously and wirelessly, Nat. Commun. 13 (1) (2022) 7259.
- [82] Y.R. Lewis-Israeli, et al., Self-assembling human heart organoids for the modeling of cardiac development and congenital heart disease, Nat. Commun. 12 (1) (2021) 5142.
- [83] J.M. Githaka, et al., BAD regulates mammary gland morphogenesis by 4E-BP1-mediated control of localized translation in mouse and human models, Nat. Commun. 12 (1) (2021) 2939.
- [84] P.A. Fernández, et al., Surface-tension-induced budding drives alveologenesis in human mammary gland organoids, Nat. Phys. 17 (10) (2021) 1130–1136.
- [85] S. Sahu, et al., Growth factor dependency in mammary organoids regulates ductal morphogenesis during organ regeneration, Sci. Rep. 12 (1) (2022) 7200.
- [86] T. Jardé, et al., Wnt and Neuregulin1/ErbB signalling extends 3D culture of hormone responsive mammary organoids, Nat. Commun. 7 (1) (2016) 13207.
- [87] Z. Zhou, et al., An organoid-based screen for epigenetic inhibitors that stimulate antigen presentation and potentiate T-cell-mediated cytotoxicity, Nat. Biomed. Eng. 5 (11) (2021) 1320–1335.
- [88] M.J. Feigman, et al., Pregnancy reprograms the epigenome of mammary epithelial cells and blocks the development of premalignant lesions, Nat. Commun. 11 (1) (2020) 2649.
- [89] E. Prince, et al., Biomimetic hydrogel supports initiation and growth of patient-derived breast tumor organoids, Nat. Commun. 13 (1) (2022) 1466.
- [90] B.S. Beydag-Tasöz, S. Yennek, A. Grapin-Botton, Towards a better understanding of diabetes mellitus using organoid models, Nat. Rev. Endocrinol. 19 (4) (2023) 232–248.
- [91] L. Huang, et al., Ductal pancreatic cancer modeling and drug screening using human pluripotent stem cell– and patient-derived tumor organoids, Nat. Med. 21 (11) (2015) 1364–1371.
- [92] S. Randriamanantsoa, et al., Spatiotemporal dynamics of self-organized branching in pancreas-derived organoids, Nat. Commun. 13 (1) (2022) 5219.
- [93] Nat. Methods 12 (5) (2015).
- [94] I. Heo, et al., Modelling Cryptosporidium infection in human small intestinal and lung organoids, Nat. Microbiol. 3 (7) (2018) 814–823.
- [95] Y. Hu, et al., Lung cancer organoids analyzed on microwell arrays predict drug responses of patients within a week, Nat. Commun. 12 (1) (2021) 2581.

- [96] L.L.Y. Chan, et al., The establishment of COPD organoids to study host-pathogen interaction reveals enhanced viral fitness of SARS-CoV-2 in bronchi, Nat. Commun. 13 (1) (2022) 7635.
- [97] M. Kim, et al., Patient-derived lung cancer organoids as in vitro cancer models for therapeutic screening, Nat. Commun. 10 (1) (2019) 3991.
- [98] A.J. Miller, et al., Generation of lung organoids from human pluripotent stem cells in vitro, Nat. Protoc. 14 (2) (2019) 518–540.
- [99] S.L. Leibel, et al., Reversal of Surfactant Protein B Deficiency in Patient Specific Human Induced Pluripotent Stem Cell Derived Lung Organoids by Gene Therapy, Sci. Rep. 9 (1) (2019) 13450.
- [100] K. Hoffmann, et al., Human alveolar progenitors generate dual lineage bronchioalveolar organoids, Communications Biology 5 (1) (2022) 875.
- [101] M.C. Chiu, et al., A bipotential organoid model of respiratory epithelium recapitulates high infectivity of SARS-CoV-2 Omicron variant, Cell Discovery 8 (1) (2022) 57.
- [102] J.-H. Kim, et al., Human pluripotent stem cell-derived alveolar organoids for modeling pulmonary fibrosis and drug testing, Cell Death Discovery 7 (1) (2021) 48
- [103] E. Sano, et al., Cell response analysis in SARS-CoV-2 infected bronchial organoids, Communications Biology 5 (1) (2022) 516.
- [104] Calderon-Gierszal, E.L. and G.S. Prins, Prostate organoids: Directed differentiation from embryonic stem cells, in Organoids and Mini-Organs, J.A. Davies and M.L. Lawrence, Editors. 2018, Academic Press. p. 89-116.
- [105] L. Puca, et al., Patient derived organoids to model rare prostate cancer phenotypes, Nat. Commun. 9 (1) (2018) 2404.
- [106] S. Pamarthy, H.E. Sabaawy, Patient derived organoids in prostate cancer: improving therapeutic efficacy in precision medicine, Mol. Cancer 20 (1) (2021) 125
- [107] J. Drost, et al., Organoid culture systems for prostate epithelial and cancer tissue, Nat. Protoc. 11 (2) (2016) 347–358.
- [108] R. Servant, et al., Prostate cancer patient-derived organoids: detailed outcome from a prospective cohort of 81 clinical specimens, J Pathol 254 (5) (2021) 543–555
- [109] Zhou, L., et al., Application of Organoid Models in Prostate Cancer Research. 2021.
 11.
- [110] K. Cheaito, et al., Establishment and characterization of prostate organoids from treatment-naïve patients with prostate cancer, Oncol Lett 23 (1) (2022) 6.
- [111] M. Romitti, et al., Transplantable human thyroid organoids generated from embryonic stem cells to rescue hypothyroidism, Nat. Commun. 13 (1) (2022) 7057.
- [112] H. Samimi, et al., A systematic review on thyroid organoid models: time-trend and its achievements. 320 (3) (2021) E581–E590.
- [113] J. van der Vaart, et al., Adult mouse and human organoids derived from thyroid follicular cells and modeling of Graves' hyperthyroidism, Proc Natl Acad Sci U S A 118 (51) (2021).
- [114] Yang, H., et al., Establishment of papillary thyroid cancer organoid lines from clinical specimens. 2023. 14.
- [115] D. Chen, et al., Papillary thyroid cancer organoids harboring BRAFV600E mutation reveal potentially beneficial effects of BRAF inhibitor-based combination therapies, J. Transl. Med. 21 (1) (2023) 9.
- [116] Martin, A., et al., Preservation of Functioning Human Thyroid "Organoids" in the scid Mouse. IV. In Vivo Selection of an Intrathyroidal T Cell Receptor Repertoire*. Endocrinology, 1997. 138(11): p. 4868-4875.
- [117] Thyroid Gland Organoids, Current Models and Insights for Application in Tissue Engineering. 28 (11–12) (2022) 500–510.
- [118] J.L. Norrie, et al., Retinoblastoma from human stem cell-derived retinal organoids, Nat. Commun. 12 (1) (2021) 4535.
- [119] M. Völkner, et al., HBEGF-TNF induce a complex outer retinal pathology with photoreceptor cell extrusion in human organoids, Nat. Commun. 13 (1) (2022) 6183.
- [120] K. Eastlake, et al., Transcriptomics of CD29+/CD44+ cells isolated from hPSC retinal organoids reveals a single cell population with retinal progenitor and Müller glia characteristics, Sci. Rep. 13 (1) (2023) 5081.
- [121] M.K.E. Blixt, et al., MYCN induces cell-specific tumorigenic growth in RB1proficient human retinal organoid and chicken retina models of retinoblastoma, Oncogenesis 11 (1) (2022) 34.
- [122] J. Zhou, et al., Human retinal organoids release extracellular vesicles that regulate gene expression in target human retinal progenitor cells, Sci. Rep. 11 (1) (2021) 21128.
- [123] D. Agarwal, et al., Bulk RNA sequencing analysis of developing human induced pluripotent cell-derived retinal organoids, Sci. Data 9 (1) (2022) 759.
- [124] S.H. Lee, et al., Role of mTORC1 activity during early retinal development and lamination in human-induced pluripotent stem cell-derived retinal organoids, Cell Death Discovery 8 (1) (2022) 56.
- [125] D. Saengwimol, et al., A three-dimensional organoid model recapitulates tumorigenic aspects and drug responses of advanced human retinoblastoma, Sci. Rep. 8 (1) (2018) 15664.
- [126] C. Singh, S. Roy-Chowdhuri, Quantitative Real-Time PCR: Recent Advances, Methods Mol Biol 1392 (2016) 161–176.
- [127] L. Pillai-Kastoori, A.R. Schutz-Geschwender, J.A. Harford, A systematic approach to quantitative Western blot analysis, Anal Biochem 593 (2020) 113608.
- [128] M.C. Rudolph, E.A. Wellberg, S.M. Anderson, Adipose-depleted mammary epithelial cells and organoids, J Mammary Gland Biol Neoplasia 14 (4) (2009) 381, 386
- [129] M.J. Sanderson, et al., Fluorescence microscopy, 2014, Cold Spring Harb Protoc, 2014.

- [130] J.L. Regan, Immunofluorescence staining of colorectal cancer patient-derived organoids, Methods Cell Biol 171 (2022) 163–171.
- [131] J.F. Dekkers, et al., High-resolution 3D imaging of fixed and cleared organoids, Nat Protoc 14 (6) (2019) 1756–1771.
- [132] R.L. van Ineveld, et al., Single-Cell Resolution Three-Dimensional Imaging of Intact Organoids, J Vis Exp 160 (2020).
- [133] E. Karzbrun, R.Y. Tshuva, O. Reiner, An On-Chip Method for Long-Term Growth and Real-Time Imaging of Brain Organoids, Curr Protoc Cell Biol 81 (1) (2018) e62
- [134] A.W. Browne, et al., Structural and Functional Characterization of Human Stem-Cell-Derived Retinal Organoids by Live Imaging, Invest Ophthalmol Vis Sci 58 (9) (2017) 3311–3318.
- [135] H.F. Farin, et al., Visualization of a short-range Wnt gradient in the intestinal stem-cell niche, Nature 530 (7590) (2016) 340–343.
- [136] M.A. Basson, Signaling in cell differentiation and morphogenesis, 4, Cold Spring Harb Perspect Biol, 2012.
- [137] K.H. Vining, D.J. Mooney, Mechanical forces direct stem cell behaviour in development and regeneration, Nat Rev Mol Cell Biol 18 (12) (2017) 728–742.
- [138] V.D.L. Putra, K.A. Kilian, M.L. Knothe Tate, Biomechanical, biophysical and biochemical modulators of cytoskeletal remodelling and emergent stem cell lineage commitment, Communications Biology 6 (1) (2023) 75.
- [139] J.A. Brassard, M.P. Lutolf, Engineering Stem Cell Self-organization to Build Better Organoids, Cell Stem Cell 24 (6) (2019) 860–876.
- [140] M.R. Blatchley, K.S. Anseth, Middle-out methods for spatiotemporal tissue engineering of organoids, Nature Reviews Bioengineering 1 (5) (2023) 329–345.
- [141] C. Mandrycky, et al., 3D bioprinting for engineering complex tissues, Biotechnol Adv 34 (4) (2016) 422–434.
- [142] H. Ravanbakhsh, et al., Emerging Technologies in Multi-Material Bioprinting. 33 (49) (2021) 2104730.
- [143] M.A. Heinrich, et al., 3D Bioprinting: from Benches to Translational Applications, Small 15 (23) (2019) e1805510.
- [144] A.C. Daly, M.D. Davidson, J.A. Burdick, 3D bioprinting of high cell-density heterogeneous tissue models through spheroid fusion within self-healing hydrogels, Nat. Commun. 12 (1) (2021) 753.
- [145] T.Y. Kim, et al., Directed fusion of cardiac spheroids into larger heterocellular microtissues enables investigation of cardiac action potential propagation via cardiac fibroblasts, PLoS One 13 (5) (2018) e0196714.
- [146] A.C. Rios, H. Clevers, Imaging organoids: a bright future ahead, Nat. Methods 15 (1) (2018) 24–26.
- [147] X. Qian, et al., Brain-Region-Specific Organoids Using Mini-bioreactors for Modeling ZIKV Exposure, Cell 165 (5) (2016) 1238–1254.
- [148] Xue, Y., et al., Retinal Organoids Long-Term Functional Characterization Using Two-Photon Fluorescence Lifetime and Hyperspectral Microscopy, 2021. 15
- Photon Fluorescence Lifetime and Hyperspectral Microscopy. 2021. 15.
 [149] B.C. Chen, et al., Lattice light-sheet microscopy: imaging molecules to embryos at
- high spatiotemporal resolution, Science 346 (6208) (2014) 1257998.

 [150] A. Bodén, et al., Volumetric live cell imaging with three-dimensional parallelized
- RESOLFT microscopy, Nat. Biotechnol. 39 (5) (2021) 609–618. [151] K. Han, et al., 3D super-resolution live-cell imaging with radial symmetry and
- Fourier light-field microscopy, Biomed. Opt. Express 13 (11) (2022) 5574–5584. [152] H. Schneckenburger, et al., Novel Approaches in 3D Live Cell Microscopy. in 2022
- International Conference Laser Optics (ICLO), 2022.
 [153] I. Lukonin, et al., Phenotypic landscape of intestinal organoid regeneration,
- 155] I. Lukolini, et al., Phenotypic landscape of intestinal organoid regeneration, Nature 586 (7828) (2020) 275–280.
- [154] A.H. Zewail, Four-dimensional electron microscopy, Science 328 (5975) (2010) 187–193.
- [155] N. Sachs, et al., Long-term expanding human airway organoids for disease modeling, EMBO J. 38 (4) (2019) e100300.
- [156] F. Schutgens, et al., Tubuloids derived from human adult kidney and urine for personalized disease modeling, Nat. Biotechnol. 37 (3) (2019) 303–313.
- [157] J.N.T. Nguyen, A.M. Harbison, Scanning electron microscopy sample preparation and imaging, in: Molecular Profiling, Springer, 2017, pp. 71–84.
- [158] A.S. Monzel, et al., Derivation of human midbrain-specific organoids from neuroepithelial stem cells, Stem Cell Rep. 8 (5) (2017) 1144–1154.
- [159] V. Iefremova, et al., An organoid-based model of cortical development identifies non-cell-autonomous defects in Wnt signaling contributing to Miller-Dieker syndrome, Cell Rep. 19 (1) (2017) 50–59.
- [160] A.A. Sivitilli, et al., Robust production of uniform human cerebral organoids from pluripotent stem cells, Life Sci Alliance 3 (5) (2020).
- [161] A. Sivitilli, P. Ghiasi, L. Attisano, Production of phenotypically uniform human cerebral organoids from pluripotent stem cells, Bio-protocol 11 (8) (2021) e3985–e.
- [162] E.E. Capowski, et al., Reproducibility and staging of 3D human retinal organoids across multiple pluripotent stem cell lines, Development 146 (1) (2019).
- [163] J.-M.-F. Martins, et al., Self-organizing 3D human trunk neuromuscular organoids, Cell Stem Cell 26 (2) (2020).
- [164] T. Kassis, et al., OrgaQuant: human intestinal organoid localization and quantification using deep convolutional neural networks, Sci. Rep. 9 (1) (2019) 12479.
- [165] J.M. Matthews, et al., OrganoID: A versatile deep learning platform for tracking and analysis of single-organoid dynamics, PLoS Comput. Biol. 18 (11) (2022) e1010584
- [166] E. Domènech-Moreno, et al., Tellu-an object-detector algorithm for automatic classification of intestinal organoids, Dis. Model. Mech. 16 (3) (2023).
- [167] K. Fei, et al., Present Application and Perspectives of Organoid Imaging Technology, Bioengineering 9 (3) (2022) 121.

- [168] J.W. Lichtman, J.-A. Conchello, Fluorescence microscopy, Nat. Methods 2 (12) (2005) 910–919.
- [169] N. Sachs, et al., A living biobank of breast cancer organoids captures disease heterogeneity, Cell 172 (1) (2018).
- [170] B. Huang, M. Bates, X. Zhuang, Super-resolution fluorescence microscopy, Annu Rev Biochem 78 (2009) 993–1016.
- [171] A. Ettinger, T. Wittmann, Fluorescence live cell imaging, Methods Cell Biol 123 (2014) 77–94.
- [172] R. Hoebe, et al., Controlled light-exposure microscopy reduces photobleaching and phototoxicity in fluorescence live-cell imaging, Nat. Biotechnol. 25 (2) (2007) 249–253.
- [173] C. Bremond Martin, et al., Recent Trends and Perspectives in Cerebral Organoids Imaging and Analysis, Front. Neurosci. (2021) 717.
- [174] P.R. Jamieson, et al., Derivation of a robust mouse mammary organoid system for studying tissue dynamics, Development 144 (6) (2017) 1065–1071.
- [175] N.P. Tallapragada, et al., Inflation-collapse dynamics drive patterning and morphogenesis in intestinal organoids, Cell Stem Cell 28 (9) (2021).
- [176] G. Martínez-Ara, et al., Optogenetic control of apical constriction induces synthetic morphogenesis in mammalian tissues, Nat. Commun. 13 (1) (2022) 1.13
- [177] E. Gratton, et al., Multiphoton fluorescence microscopy, Methods 25 (1) (2001) 103–110.
- [178] C.J. Sheppard, Multiphoton microscopy: a personal historical review, with some future predictions, J. Biomed. Opt. 25 (1) (2020) 014511.
- [179] Y. Xue, et al., Retinal organoids long-term functional characterization using twophoton fluorescence lifetime and hyperspectral microscopy, Front. Cell. Neurosci. 15 (2021) 796903.
- [180] M. Yildirim, et al., Label-free three-photon imaging of intact human cerebral organoids for tracking early events in brain development and deficits in Rett syndrome, Elife 11 (2022) e78079.
- [181] A. Hashmi, et al., Cell-state transitions and collective cell movement generate an endoderm-like region in gastruloids, Elife 11 (2022) e59371.
- [182] M. Barroso, et al., Probing organoid metabolism using Fluorescence Lifetime Imaging Microscopy (FLIM): the next frontier of drug discovery and disease understanding, Adv. Drug Deliv. Rev. (2023) 115081.
- [183] L. Becker, et al., Data-driven identification of biomarkers for in situ monitoring of drug treatment in bladder cancer organoids, Int. J. Mol. Sci. 23 (13) (2022) 6956.
- [184] I.A. Okkelman, et al., Use of Fluorescence Lifetime Imaging Microscopy (FLIM) as a Timer of Cell Cycle S Phase, PLoS One 11 (12) (2016) e0167385.
- [185] I.A. Okkelman, et al., Live cell imaging of mouse intestinal organoids reveals heterogeneity in their oxygenation, Biomaterials 146 (2017) 86–96.
- [186] P.H. Lakner, et al., Applying phasor approach analysis of multiphoton FLIM measurements to probe the metabolic activity of three-dimensional in vitro cell culture models, Sci. Rep. 7 (1) (2017) 42730.
- [187] K. Chatterjee, et al., Recent progress in light sheet microscopy for biological applications, Appl. Spectrosc. 72 (8) (2018) 1137–1169.
- [188] E.G. Reynaud, et al., Guide to light-sheet microscopy for adventurous biologists, Nat. Methods 12 (1) (2015) 30–34.
- [189] P. Delgado-Rodriguez, et al., Innovations in ex vivo light sheet fluorescence microscopy, Prog. Biophys. Mol. Biol. 168 (2022) 37–51.
- [190] J. Huisken, et al., Optical sectioning deep inside live embryos by selective plane illumination microscopy, Science 305 (5686) (2004) 1007–1009.
- [191] G. de Medeiros, et al., Multiscale light-sheet organoid imaging framework, Nat. Commun. 13 (1) (2022) 4864.
- [192] Beydag-Tasöz, B.S., et al., A combined transcriptional and dynamic roadmap of single human pancreatic endocrine progenitors reveals proliferative capacity and differentiation continuum. bioRxiv, 2021.
- [193] Z. He, et al., Lineage recording in human cerebral organoids, Nat. Methods 19 (1) (2022) 90–99.
- [194] L. Hof, et al., Long-term live imaging and multiscale analysis identify heterogeneity and core principles of epithelial organoid morphogenesis, BMC Biol. 19 (1) (2021) 37.
- [195] T.A. Planchon, et al., Rapid three-dimensional isotropic imaging of living cells using Bessel beam plane illumination, Nat. Methods 8 (5) (2011) 417–423.
- [196] J. Schöneberg, et al., 4D cell biology: big data image analytics and lattice light-sheet imaging reveal dynamics of clathrin-mediated endocytosis in stem cell-derived intestinal organoids, Mol. Biol. Cell 29 (24) (2018) 2959–2968.
- [197] Medeiros, G.d., et al., Confocal multiview light-sheet microscopy. Nature communications, 2015. 6(1): p. 1-8.
- [198] L. Hof, et al., Long-term live imaging and multiscale analysis identify heterogeneity and core principles of epithelial organoid morphogenesis, BMC Biol. 19 (1) (2021) 1–22.
- [199] K. McDole, et al., In toto imaging and reconstruction of post-implantation mouse development at the single-cell level, Cell 175 (3) (2018).
- [200] P. Strnad, et al., Inverted light-sheet microscope for imaging mouse preimplantation development, Nat. Methods 13 (2) (2016) 139–142.
- [201] G. Rossi, et al., Capturing cardiogenesis in gastruloids, Cell Stem Cell 28 (2) (2021).
- [202] D. Serra, et al., Self-organization and symmetry breaking in intestinal organoid development, Nature 569 (7754) (2019) 66–72.
 [203] Q. Yang, et al., Cell fate coordinates mechano-osmotic forces in intestinal crypt
- formation, Nat. Cell Biol. 23 (7) (2021) 733–744. $\hbox{\bf [204] Y. Liu, et al., Amplified stimulated emission in upconversion nanoparticles for the context of the context of$
- super-resolution nanoscopy, Nature 543 (7644) (2017) 229–233. [205] P.R. Ormel, et al., Microglia innately develop within cerebral organoids, Nat.
- [205] P.R. Ormel, et al., Microglia innately develop within cerebral organoids, Na Commun. 9 (1) (2018) 4167.

- [206] J.J. Poole, L.B. Mostaço-Guidolin, Optical microscopy and the extracellular matrix structure: a review, Cells 10 (7) (2021) 1760.
- [207] M.J. Rust, M. Bates, X. Zhuang, Sub-diffraction-limit imaging by stochastic optical reconstruction microscopy (STORM), Nat. Methods 3 (10) (2006) 793–796.
- [208] Q.P. Su, L.A. Ju, Biophysical nanotools for single-molecule dynamics, Biophys. Rev. 10 (5) (2018) 1349–1357.
- [209] E. Wilson, W. Knudson, K. Newell-Litwa, Hyaluronan regulates synapse formation and function in developing neural networks, Sci Rep 10 (1) (2020) 16459.
- [210] S. Marschall, et al., Optical coherence tomography—current technology and applications in clinical and biomedical research, Anal. Bioanal. Chem. 400 (9) (2011) 2699–2720.
- [211] S.A. Boppart, et al., In vivo cellular optical coherence tomography imaging, Nat. Med. 4 (7) (1998) 861–865.
- [212] T. Otani, Y. Yamaguchi, S. Kishi, Improved visualization of Henle fiber layer by changing the measurement beam angle on optical coherence tomography, Retina 31 (3) (2011) 497–501.
- [213] D.A. Gil, D.A. Deming, M.C. Skala, Volumetric growth tracking of patient-derived cancer organoids using optical coherence tomography, Biomed. Opt. Express 12 (7) (2021) 3789–3805.
- [214] Y. Ming, et al., Longitudinal morphological and functional characterization of human heart organoids using optical coherence tomography, Biosens. Bioelectron. 207 (2022) 114136.
- [215] J. Scholler, et al., Dynamic full-field optical coherence tomography: 3D liveimaging of retinal organoids, Light Sci. Appl. 9 (1) (2020) 140.
- [216] J. Xia, J. Yao, L.V. Wang, Photoacoustic tomography: principles and advances, Electromagn Waves (Camb) 147 (2014) 1–22.
- [217] S. Roberts, et al., Calcium sensor for photoacoustic imaging, J. Am. Chem. Soc. 140 (8) (2018) 2718–2721.
- [218] G. Obaid, et al., Impacting pancreatic cancer therapy in heterotypic in vitro organoids and in vivo tumors with specificity-tuned, NIR-activable photoimmunonanoconjugates: towards conquering desmoplasia? Nano Lett. 19 (11) (2019) 7573–7587.
- [219] C. Ma, et al., Photoacoustic imaging of 3D-printed vascular networks, Biofabrication 14 (2) (2022) 025001.
- [220] A. Neprokin, et al., Photoacoustic Imaging in Biomedicine and Life Sciences, Life (Basel) 12 (4) (2022).
- [221] M.B. Bouchard, et al., Swept confocally-aligned planar excitation (SCAPE) microscopy for high-speed volumetric imaging of behaving organisms, Nat. Photonics 9 (2) (2015) 113–119.
- [222] R. Prevedel, et al., Brillouin microscopy: an emerging tool for mechanobiology, Nat. Methods 16 (10) (2019) 969–977.
- [223] K. Dodo, K. Fujita, M. Sodeoka, Raman Spectroscopy for Chemical Biology Research. J. Am. Chem. Soc. 144 (43) (2022) 19651–19667.
- [224] W. Mao, et al., Spectroscopic Techniques for Monitoring Stem Cell and Organoid Proliferation in 3D environments for Therapeutic Development, Adv. Drug Deliv. Rev. (2023) 115074.
- [225] M. Urbanczyk, et al., Decorin improves human pancreatic β-cell function and regulates ECM expression in vitro, Matrix Biol. 115 (2023) 160–183.
- [226] A. Zbinden, et al., Non-invasive marker-independent high content analysis of a microphysiological human pancreas-on-a-chip model, Matrix Biol. 85 (2020) 205–220.
- [227] S.J. Edwards, et al., High-resolution imaging of tumor spheroids and organoids enabled by expansion microscopy, Front. Mol. Biosci. 7 (2020) 208.
- [228] M.R. Blatchley, et al., In situ super-resolution imaging of organoids and extracellular matrix interactions via phototransfer by allyl sulfide exchangeexpansion microscopy (PhASE-ExM), Adv. Mater. 34 (16) (2022) 2109252.
- [229] C. Haase, et al., Image-seq: spatially resolved single-cell sequencing guided by in situ and in vivo imaging, Nat. Methods 19 (12) (2022) 1622–1633.
- [230] P. Wahle, et al., Multimodal spatiotemporal phenotyping of human retinal organoid development, Nat. Biotechnol. (2023) 1–11.
- [231] M.A. Ansari, et al., Diffuse optical tomography: image reconstruction and verification, J Lasers Med Sci 5 (1) (2014) 13–18.
- [232] P.W. Winter, et al., Two-photon instant structured illumination microscopy improves the depth penetration of super-resolution imaging in thick scattering samples, Optica 1 (3) (2014) 181–191.
- [233] X. Chen, et al., Superresolution structured illumination microscopy reconstruction algorithms: a review, Light Sci. Appl. 12 (1) (2023) 172.
- [234] E.C. Costa, et al., Optical clearing methods: An overview of the techniques used for the imaging of 3D spheroids, Biotechnol Bioeng 116 (10) (2019) 2742–2763.
- [235] J. Seo, M. Choe, S.-Y. Kim, Clearing and Labeling Techniques for Large-Scale Biological Tissues, Mol. Cells 39 (6) (2016) 439–446.
- [236] H. Renner, et al., Fluorescence-based Single-cell Analysis of Whole-mount-stained and Cleared Microtissues and Organoids for High Throughput Screening, Bio Protoc 11 (12) (2021) e4050.
- [237] A. Ertürk, et al., Three-dimensional imaging of solvent-cleared organs using 3DISCO, Nat. Protoc. 7 (11) (2012) 1983–1995.
- [238] N. Renier, et al., iDISCO: a simple, rapid method to immunolabel large tissue samples for volume imaging, Cell 159 (4) (2014) 896–910.
- [239] T.C. Murakami, et al., A three-dimensional single-cell-resolution whole-brain atlas using CUBIC-X expansion microscopy and tissue clearing, Nat. Neurosci. 21 (4) (2018) 625–637.
- [240] R. Tomer, et al., Advanced CLARITY for rapid and high-resolution imaging of intact tissues, Nat. Protoc. 9 (7) (2014) 1682–1697.
- [241] S.V. Murphy, A. Atala, 3D bioprinting of tissues and organs, Nat Biotechnol 32 (8) (2014) 773–785.

- [242] Y.S. Zhang, et al., 3D Bioprinting for Tissue and Organ Fabrication, Ann Biomed Eng 45 (1) (2017) 148–163.
- [243] E.J. Reed, et al., Biomimicry as a route to new materials: what kinds of lessons are useful? Philos Trans A Math Phys Eng Sci 2009 (367) (1893) 1571–1585.
- [244] Y.S. Zhang, et al., 3D extrusion bioprinting, Nature Reviews Methods Primers 1 (1) (2021) 75.
- [245] S. Ramesh, et al., Extrusion bioprinting: Recent progress, challenges, and future opportunities, Bioprinting 21 (2021) e00116.
- [246] L. Lian, et al., Uniaxial and Coaxial Vertical Embedded Extrusion Bioprinting. 11 (9) (2022) 2102411.
- [247] T. Xu, et al., Complex heterogeneous tissue constructs containing multiple cell types prepared by inkjet printing technology, Biomaterials 34 (1) (2013) 130–139.
- [248] A. Negro, T. Cherbuin, M.P. Lutolf, 3D Inkjet Printing of Complex, Cell-Laden Hydrogel Structures, Sci. Rep. 8 (1) (2018) 17099.
- [249] J.A. Park, et al., Freeform micropatterning of living cells into cell culture medium using direct inkjet printing, Sci. Rep. 7 (1) (2017) 14610.
- [250] M. Xie, et al., Volumetric additive manufacturing of pristine silk-based (bio)inks, Nat. Commun. 14 (1) (2023) 210.
- [251] M. Wang, et al., Molecularly cleavable bioinks facilitate high-performance digital light processing-based bioprinting of functional volumetric soft tissues, Nat. Commun. 13 (1) (2022) 3317.
- [252] Z. Zheng, et al., Visible Light-Induced 3D Bioprinting Technologies and Corresponding Bioink Materials for Tissue Engineering: A Review, Engineering 7 (7) (2021) 966–978.
- [253] W. Li, et al., Stereolithography apparatus and digital light processing-based 3D bioprinting for tissue fabrication, iScience 26 (2) (2023) 106039.
- [254] V. Yusupov, et al., Laser-induced Forward Transfer Hydrogel Printing: A Defined Route for Highly Controlled Process, Int J Bioprint 6 (3) (2020) 271.
- [255] V. Keriquel, et al., In situ printing of mesenchymal stromal cells, by laser-assisted bioprinting, for in vivo bone regeneration applications, Sci. Rep. 7 (1) (2017) 1778.
- [256] O. Kérourédan, et al., Magnetic Resonance Imaging for tracking cellular patterns obtained by Laser-Assisted Bioprinting, Sci. Rep. 8 (1) (2018) 15777.
- [257] D.M. Kingsley, et al., Laser-based 3D bioprinting for spatial and size control of tumor spheroids and embryoid bodies, Acta Biomater 95 (2019) 357–370.
- [258] A. Zennifer, A. Subramanian, S. Sethuraman, Design considerations of bioinks for laser bioprinting technique towards tissue regenerative applications, Bioprinting 27 (2022) e00205.
- [259] N.I. Moldovan, N. Hibino, K. Nakayama, Principles of the Kenzan Method for Robotic Cell Spheroid-Based Three-Dimensional Bioprinting
 sup/>, Tissue Eng
 Part B Rev 23 (3) (2017) 237–244.
- [260] C.S. Ong, I. Pitaktong, N. Hibino, Principles of Spheroid Preparation for Creation of 3D Cardiac Tissue Using Biomaterial-Free Bioprinting, Methods Mol Biol 2140 (2020) 183–197.
- [261] J. Yu, et al., Current Advances in 3D Bioprinting Technology and Its Applications for Tissue Engineering, Polymers (Basel) 12 (12) (2020).
- [262] M. Askari, et al., Recent progress in extrusion 3D bioprinting of hydrogel biomaterials for tissue regeneration: a comprehensive review with focus on advanced fabrication techniques, Biomater Sci 9 (3) (2021) 535–573.
- [263] N. Betancourt, X. Chen, Review of extrusion-based multi-material bioprinting processes, Bioprinting 25 (2022) e00189.
- [264] A. Schwab, et al., Printability and Shape Fidelity of Bioinks in 3D Bioprinting, Chem. Rev. 120 (19) (2020) 11028–11055.
- [265] D. Wang, et al., Microfluidic bioprinting of tough hydrogel-based vascular conduits for functional blood vessels. 8 (43) (2022).
- [266] Q. Pi, et al., Digitally Tunable Microfluidic Bioprinting of Multilayered Cannular Tissues. 30 (43) (2018) 1706913.
- [267] G. Tang, et al., Liquid-embedded (bio)printing of alginate-free, standalone, ultrafine, and ultrathin-walled cannular structures, Proc Natl Acad Sci U S A 120 (7) (2023).
- [268] W. Jia, et al., Direct 3D bioprinting of perfusable vascular constructs using a blend bioink, Biomaterials 106 (2016) 58–68.
- [269] L. Cheng, et al., A 3D Bioprinted Gut Anaerobic Model for Studying Bacteria– Host Interactions. 6 (2023) 0058.
- [270] D. Wu, et al., A 3D-Bioprinted Multiple Myeloma Model. 11 (7) (2022) 2100884.
- [271] Y. Sun, et al., 3D bioprinting dual-factor releasing and gradient-structured constructs ready to implant for anisotropic cartilage regeneration. 6 (37) (2020).
- [272] O. Messaoudi, et al., Stem Cells and Extrusion 3D Printing for Hyaline Cartilage Engineering, Cells 10 (1) (2020).
- [273] A. McCormack, et al., 3D Printing in Suspension Baths: Keeping the Promises of Bioprinting Afloat, Trends Biotechnol 38 (6) (2020) 584–593.
- [274] X. Zeng, et al., Embedded bioprinting for designer 3D tissue constructs with complex structural organization, Acta Biomater. 140 (2022) 1–22.
- [275] M. Rocca, et al., Embedded Multimaterial Extrusion Bioprinting, SLAS Technol 23 (2) (2018) 154–163.
- [276] T.J. Hinton, et al., Three-dimensional printing of complex biological structures by freeform reversible embedding of suspended hydrogels, Sci Adv 1 (9) (2015) e1500758.
- [277] M.R. Williamson, et al., The role of endothelial cell attachment to elastic fibre molecules in the enhancement of monolayer formation and retention, and the inhibition of smooth muscle cell recruitment, Biomaterials 28 (35) (2007) 5307–5318.
- [278] S. Lee, et al., Human-Recombinant-Elastin-Based Bioinks for 3D Bioprinting of Vascularized Soft Tissues, Adv Mater 32 (45) (2020) e2003915.

- [279] E.M. Shen, K.E. McCloskey, Affordable, high-resolution bioprinting with embedded concentration gradients, Bioprinting 21 (2021) e00113.
- [280] B.S. Kim, et al., Decellularized Extracellular Matrix-based Bioinks for Engineering Tissue- and Organ-specific Microenvironments, Chem Rev 120 (19) (2020) 10608–10661.
- [281] A. Shapira, et al., Transparent support media for high resolution 3D printing of volumetric cell-containing ECM structures, Biomed Mater 15 (4) (2020) 045018.
- [282] E. Mirdamadi, et al., Agarose Slurry as a Support Medium for Bioprinting and Culturing Freestanding Cell-Laden Hydrogel Constructs 6 (2019) 158–164, 3D.
- [283] L. Shi, et al., Dynamic Coordination Chemistry Enables Free Directional Printing of Biopolymer Hydrogel, Chem. Mater. 29 (14) (2017) 5816–5823.
- [284] A.M. Compaan, K. Song, Y. Huang, Gellan Fluid Gel as a Versatile Support Bath Material for Fluid Extrusion Bioprinting, ACS Appl Mater Interfaces 11 (6) (2019) 5714–5726.
- [285] W. Wu, A. DeConinck, J.A. Lewis, Omnidirectional printing of 3D microvascular networks, Adv Mater 23 (24) (2011) H178–H183.
- [286] W. Cheng, et al., Granular hydrogels for 3D bioprinting applications. 1 (3) (2020) 20200060.
- [287] A.C. Daly, et al., Hydrogel microparticles for biomedical applications, Nat Rev Mater 5 (1) (2020) 20–43.
- [288] A.M. Compaan, et al., Cross-Linkable Microgel Composite Matrix Bath for Embedded Bioprinting of Perfusable Tissue Constructs and Sculpting of Solid Objects, ACS Appl Mater Interfaces 12 (7) (2020) 7855–7868.
- [289] Y. Jin, et al., Functional Nanoclay Suspension for Printing-Then-Solidification of Liquid Materials, ACS Appl Mater Interfaces 9 (23) (2017) 20057–20066.
- [290] A. Lee, et al., 3D bioprinting of collagen to rebuild components of the human heart, Science 365 (6452) (2019) 482–487.
- [291] D.M. Hobbs, F.J. Muzzio, The Kenics static mixer: a three-dimensional chaotic flow, Chem. Eng. J. 67 (3) (1997) 153–166.
- [292] C. Chávez-Madero, et al., Using chaotic advection for facile high-throughput fabrication of ordered multilayer micro- and nanostructures: continuous chaotic printing, Biofabrication 12 (3) (2020) 035023.
- [293] Meijer, H.E., M.K. Singh, and P.D.J.P.i.p.s. Anderson, On the performance of static mixers: A quantitative comparison. 2012. 37(10): p. 1333-1349.
- [294] G. Trujillo-de Santiago, et al., Chaotic printing: using chaos to fabricate densely packed micro- and nanostructures at high resolution and speed, Mater. Horiz. 5 (5) (2018) 813–822.
- [295] C.F. Ceballos-González, et al., High-Throughput and Continuous Chaotic Bioprinting of Spatially Controlled Bacterial Microcosms, ACS Biomater Sci Eng 7 (6) (2021) 2408–2419.
- [296] X. Jiang, N. Yang, R. Wang, Effect of Aspect Ratio on the Mixing Performance in the Kenics Static Mixer. 9 (3) (2021) 464.
- [297] A.I. Frías-Sánchez, et al., Biofabrication of muscle fibers enhanced with plant viral nanoparticles using surface chaotic flows, Biofabrication 13 (3) (2021).
- [298] E.J. Bolívar-Monsalve, et al., Continuous chaotic bioprinting of skeletal musclelike constructs, Bioprinting 21 (2021) e00125.
- [299] E.J. Bolívar-Monsalve, et al., One-Step Bioprinting of Multi-Channel Hydrogel Filaments Using Chaotic Advection: Fabrication of Pre-Vascularized Muscle-Like Tissues, Adv Healthc Mater 11 (24) (2022) e2200448.
- [300] X. Li, et al., Inkjet Bioprinting of Biomaterials, Chem. Rev. 120 (19) (2020) 10793–10833.
- [301] F. Loffredo, et al., Bubble-Patterned Films by Inkjet Printing and Gas Foaming. 12 (6) (2022) 806.
- [302] H. Gudapati, M. Dey, I. Ozbolat, A comprehensive review on droplet-based bioprinting: Past, present and future, Biomaterials 102 (2016) 20–42.
- [303] X. Cui, et al., Thermal inkjet printing in tissue engineering and regenerative medicine, Recent Pat Drug Deliv Formul 6 (2) (2012) 149–155.
- [304] T. Xu, et al., Inkjet printing of viable mammalian cells, Biomaterials 26 (1) (2005) 93–99.
- [305] R.E. Saunders, J.E. Gough, B. Derby, Delivery of human fibroblast cells by piezoelectric drop-on-demand inkjet printing, Biomaterials 29 (2) (2008) 193–203.
- [306] Y. Gu, et al., Chitosan surface enhances the mobility, cytoplasm spreading, and phagocytosis of macrophages, Colloids Surf. B Biointerfaces 117 (2014) 42–50.
- [307] R. Suntivich, et al., Inkjet Printing of Silk Nest Arrays for Cell Hosting, Biomacromolecules 15 (4) (2014) 1428–1435.
- [308] G. Gao, et al., Inkjet-bioprinted acrylated peptides and PEG hydrogel with human mesenchymal stem cells promote robust bone and cartilage formation with minimal printhead clogging, Biotechnol J 10 (10) (2015) 1568–1577.
- [309] X. Cui, et al., Cell damage evaluation of thermal inkjet printed Chinese hamster ovary cells. 106 (6) (2010) 963–969.
- [310] T. Xu, et al., Fabrication and characterization of bio-engineered cardiac pseudo tissues, Biofabrication 1 (3) (2009) 035001.
- [311] X. Cui, T. Boland, Human microvasculature fabrication using thermal inkjet printing technology, Biomaterials 30 (31) (2009) 6221–6227.
- [312] X. Cui, et al., Direct human cartilage repair using three-dimensional bioprinting technology, Tissue Eng Part A 18 (11–12) (2012) 1304–1312.
- [313] N.A. Chartrain, C.B. Williams, A.R. Whittington, A review on fabricating tissue scaffolds using vat photopolymerization, Acta Biomater 74 (2018) 90–111.
- [314] W. Li, et al., Recent Advances in Formulating and Processing Biomaterial Inks for Vat Polymerization-Based 3D Printing, Adv Healthc Mater 9 (15) (2020) e2000156.
- [315] R. Levato, et al., Light-based vat-polymerization bioprinting, Nature Reviews Methods Primers 3 (1) (2023) 47.

- [316] C.A. Murphy, K.S. Lim, T.B.F. Woodfield, Next Evolution in Organ-Scale Biofabrication: Bioresin Design for Rapid High-Resolution Vat Polymerization. 34 (20) (2022) 2107759.
- [317] S. Krishnamoorthy, et al., Investigation of gelatin methacrylate working curves in dynamic optical projection stereolithography of vascular-like constructs, Eur. Polym. J. 124 (2020) 109487.
- [318] Z. Wang, et al., A simple and high-resolution stereolithography-based 3D bioprinting system using visible light crosslinkable bioinks, Biofabrication 7 (4) (2015) 045009.
- [319] Z. Wang, et al., Visible Light Photoinitiation of Cell-Adhesive Gelatin Methacryloyl Hydrogels for Stereolithography 3D Bioprinting, ACS Appl Mater Interfaces 10 (32) (2018) 26859–26869.
- [320] H. Kim, et al., Light-Activated Decellularized Extracellular Matrix-Based Bioinks for Volumetric Tissue Analogs at the Centimeter Scale. 31 (32) (2021) 2011252.
- [321] B. Grigoryan, et al., Multivascular networks and functional intravascular topologies within biocompatible hydrogels, Science 364 (6439) (2019) 458–464.
- [322] K.S. Lim, et al., Bio-resin for high resolution lithography-based biofabrication of complex cell-laden constructs, Biofabrication 10 (3) (2018) 034101.
- [323] A.P. Zhang, et al., Rapid fabrication of complex 3D extracellular microenvironments by dynamic optical projection stereolithography, Adv Mater 24 (31) (2012) 4266–4270.
- [324] J. Huh, et al., Combinations of photoinitiator and UV absorber for cell-based digital light processing (DLP) bioprinting, Biofabrication 13 (3) (2021).
- [325] H. Goodarzi Hosseinabadi, et al., Digital Light Processing Bioprinting Advances for Microtissue Models, ACS Biomater Sci Eng 8 (4) (2022) 1381–1395.
- [326] Y. Lu, et al., A digital micro-mirror device-based system for the microfabrication of complex, spatially patterned tissue engineering scaffolds, J Biomed Mater Res A 77 (2) (2006) 396–405.
- [327] X. Ma, et al., Deterministically patterned biomimetic human iPSC-derived hepatic model via rapid 3D bioprinting, Proc Natl Acad Sci U S A 113 (8) (2016) 2206–2211.
- [328] H. Hong, et al., Digital light processing 3D printed silk fibroin hydrogel for cartilage tissue engineering, Biomaterials 232 (2020) 119679.
- [329] S.A. Bencherif, et al., Influence of the degree of methacrylation on hyaluronic acid hydrogels properties, Biomaterials 29 (12) (2008) 1739–1749.
- [330] K.E. Drzewiecki, et al., A thermoreversible, photocrosslinkable collagen bio-ink for free-form fabrication of scaffolds for regenerative medicine, Technology (Singap World Sci) 5 (4) (2017) 185–195.
- [331] S.H. Kim, et al., Precisely printable and biocompatible silk fibroin bioink for digital light processing 3D printing, Nat Commun 9 (1) (2018) 1620.
- [332] P.N. Bernal, et al., Volumetric Bioprinting of Complex Living-Tissue Constructs within Seconds. 31 (42) (2019) 1904209.
- [333] R. Rizzo, et al., Optimized Photoclick (Bio)Resins for Fast Volumetric Bioprinting. 33 (49) (2021) 2102900.
- [334] J. Gehlen, et al., Tomographic volumetric bioprinting of heterocellular bone-like tissues in seconds, Acta Biomater. 156 (2023) 49–60.
- [335] P.N. Bernal, et al., Volumetric Bioprinting of Organoids and Optically Tuned Hydrogels to Build Liver-Like Metabolic Biofactories. 34 (15) (2022) 2110054.
- [336] F. Guillemot, et al., Laser-assisted cell printing: principle, physical parameters versus cell fate and perspectives in tissue engineering, Nanomedicine (Lond) 5 (3) (2010) 507–515.
- [337] J.A. Barron, D.B. Krizman, B.R. Ringeisen, Laser printing of single cells: statistical analysis, cell viability, and stress, Ann Biomed Eng 33 (2) (2005) 121–130.
- [338] B. Hopp, et al., Survival and proliferative ability of various living cell types after laser-induced forward transfer, Tissue Eng 11 (11–12) (2005) 1817–1823.
- [339] B. Guillotin, et al., Laser assisted bioprinting of engineered tissue with high cell density and microscale organization, Biomaterials 31 (28) (2010) 7250–7256.
- [340] J.A. Barron, et al., Biological laser printing: a novel technique for creating heterogeneous 3-dimensional cell patterns, Biomed Microdevices 6 (2) (2004) 139–147.
- [341] S. Michael, et al., Tissue engineered skin substitutes created by laser-assisted bioprinting form skin-like structures in the dorsal skin fold chamber in mice, PLoS One 8 (3) (2013) e57741.
- [342] F. Kawecki, et al., Self-assembled human osseous cell sheets as living biopapers for the laser-assisted bioprinting of human endothelial cells, Biofabrication 10 (3) (2018) 035006.
- [343] F. Guillemot, et al., High-throughput laser printing of cells and biomaterials for tissue engineering, Acta Biomater 6 (7) (2010) 2494–2500.
- [344] R. Gaebel, et al., Patterning human stem cells and endothelial cells with laser printing for cardiac regeneration, Biomaterials 32 (35) (2011) 9218–9230.
- [345] S. Tortorella, et al., Laser Assisted Bioprinting of laminin on biodegradable PLGA substrates: Effect on neural stem cell adhesion and differentiation, Bioprinting 26 (2022) e00194.
- [346] B.R. Ringeisen, et al., Laser printing of pluripotent embryonal carcinoma cells, Tissue Eng 10 (3–4) (2004) 483–491.
- [347] L. Koch, et al., Skin tissue generation by laser cell printing, Biotechnol Bioeng 109 (7) (2012) 1855–1863.
- [348] O. Kérourédan, et al., In situ prevascularization designed by laser-assisted bioprinting: effect on bone regeneration, Biofabrication 11 (4) (2019) 045002.
- [349] A. Sorkio, et al., Human stem cell based corneal tissue mimicking structures using laser-assisted 3D bioprinting and functional bioinks, Biomaterials 171 (2018) 57–71.
- [350] I.N. Aguilar, et al., Scaffold-free Bioprinting of Mesenchymal Stem Cells with the Regenova Printer: Optimization of Printing Parameters, Bioprinting 15 (2019).
- [351] Y. Yanagi, et al., In vivo and ex vivo methods of growing a liver bud through tissue connection, Sci. Rep. 7 (1) (2017) 14085.

- [352] L. Moldovan, et al., iPSC-Derived Vascular Cell Spheroids as Building Blocks for Scaffold-Free, Biofabrication 12 (12) (2017) 1700444.
- [353] W. Sun, et al., The bioprinting roadmap, Biofabrication 12 (2) (2020) 022002.
- [354] K.T. Lawlor, et al., Cellular extrusion bioprinting improves kidney organoid reproducibility and conformation, Nat. Mater. 20 (2) (2021) 260–271.
- [355] J.A. Brassard, et al., Recapitulating macro-scale tissue self-organization through organoid bioprinting, Nat. Mater. 20 (1) (2021) 22–29.
- [356] M.A. Skylar-Scott, et al., Orthogonally induced differentiation of stem cells for the programmatic patterning of vascularized organoids and bioprinted tissues, Nat. Biomed. Eng. 6 (4) (2022) 449–462.
- [357] S. Yang, et al., In situ process monitoring and automated multi-parameter evaluation using optical coherence tomography during extrusion-based bioprinting, Addit. Manuf. 47 (2021) 102251.
- [358] J.W. Tashman, et al., In situ volumetric imaging and analysis of FRESH 3D bioprinted constructs using optical coherence tomography, Biofabrication 15 (1) (2023) 014102.